Non-linear Finite Element Analysis

of

Steel Plate Tension Members

by

Yun Ping Wang

Thesis submitted to the faculty of the

Virginia Polytechnic Institute and State University

in partial fulfillment of the requirements for the degree of

Master of Science

in

Civil Engineering

APPROVED:

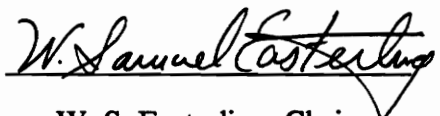

W. S. Easterling, Chairman

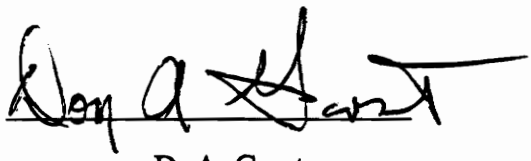

D. A. Garst

S. M. Holzer

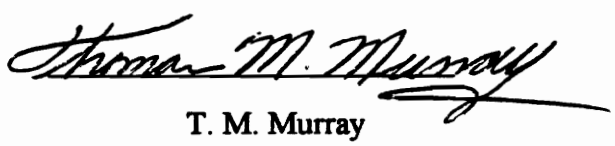

T. M. Murray

August, 1992

Blacksburg, Virginia 24061

Non-linear Finite Element Analysis

of

Steel Plate Tension Members

by

Yun Ping Wang

W. S. Easterling, Chairman

Civil Engineering

(ABSTRACT)

In the American Institute of Steel Construction (AISC) LRFD specification, the shear lag coefficient for plate members is dependent on only the ratio of the welding length to the plate width. To determine how this ratio influences the shear lag coefficient and whether there are other factors that should be considered, a finite element investigation was conducted. Experimental data from a previous study conducted at Virginia Tech was used for comparison with the analytical model.

Upon completion of the verification study, several parameters were investigated to determine their influence on the shear lag coefficient. These included the effects of weld length, eccentric load and imperfection created by the welding process. Shear lag coefficients were determined from the finite element analyses and compared with the AISC specification values.

Acknowledgements

I am truely grateful to Dr. W. Samuel Easterling for his teaching, patience and encouragement throughout this study. I would like to express my gratitude to Dr. Thomas M. Murray, Dr. Siegfried M. Holzer, and Professor Don A. Garst for their help and suggestions during the course of my study, and for serving on my committee. I am especially thankful to Dr. S. M. Holzer for allowing me use of ABAQUS as an analytical tool.

I wish to thank Dr. M. F. Feng for introducing I-DEAS, Dr. A. L. Wang for introducing fracture failure analysis, and Dr. C. W. Lu for introducing statistical convergence analysis. I also wish to thank my fellow students, Budi Widjaja and Chen Hung Wu for their lively discussions and ideas.

I thank my country (Republic of China) for providing opportunities for her officers to study and learn the precious knowledge of the world.

I am extremely indebted to my family and friends. I am especially grateful to Peter Schwartzman. I am also tremendously grateful to my parents, brothers, sisters, and my fiancee for their neverending support, without which this work would not have been possible.

Table of Contents

List of Figures

List of Tables

Chapter 1 Introduction

1.1 Background

Structural engineers have recognized the shear lag phenomenon in the design of bolted steel connections since the beginning of 1960s. Shear lag failure is described as a rupture or fracture occuring at critical sections on steel tension members due to non-uniform stress distributions created by having only part of the cross section directly connected. This phenomenon is illustrated in Fig.1-1. Because of this uneven stress distribution the strength is reduced, as compared to the full tensile strength of the member given by the product of the net area and tensile stress. With the introduction of the AISC Load and Resistance Factor Design Specifications for Structural Steel Buildings (1986), the shear lag effect was formally recognized as being applicable to welded tension members. The shear lag effect is accounted for by reducing the net area, in the case of bolted tension members, or the gross area, in the case of welded tension members, by a

factor defined as the shear lag coefficient. The effective net area, A_e, is calculated for welded tension members as:

$$A_e = UA_g$$

where A_g = gross area of member, in^2.

U = reduction coefficient = shear lag coefficient (hereafter in this study)

The effective net area is then used to compute the tensile strength.

A review of how this "***shear lag***" technology was introduced and the description of the early research may be found in report by Gonzalez and Easterling (1989). Most studies before 1986 concentrated on bolted and riveted connections because of an incorrect general idea that for welded members the gross area was equal to the effective net area. This situation did not improve until 1986 when shear lag provisions were adopted for welded members (Load and Resistance Factor Design Specifications, 1986). However, limited information on welded tension members was available, thus the weld provisions incorporated in the LRFD specification, were based on the existing criteria for bolted and riveted connections.

Due to the complexity of the shear lag problem, a reliable value of the shear lag coefficient has been difficult to obtain. Nevertheless, due to the accumulated knowledge about the essential nature of welding connections, it is gradually becoming possible to discover the solution from a variety of approaches. These approaches include experimental tests, continuous mathematical modeling , and Finite Element modeling.

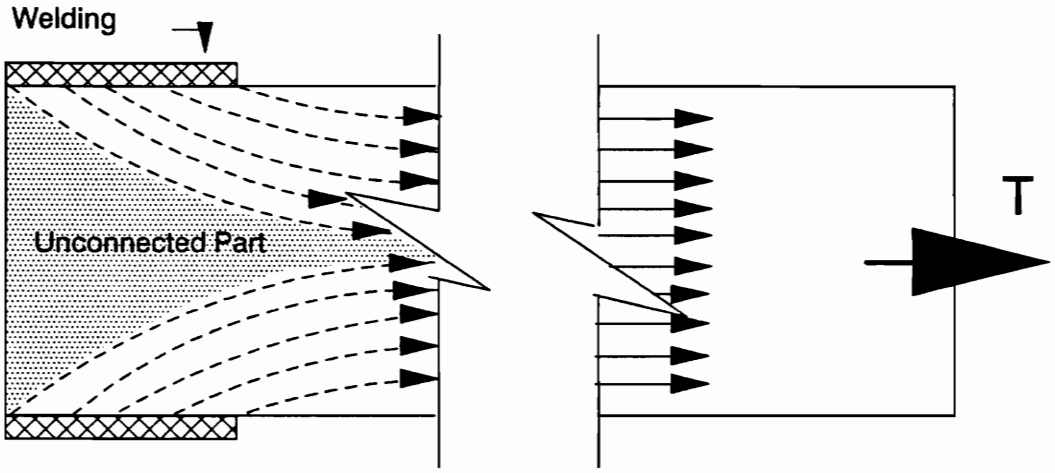

Figure 1-1 A Case of Shear Lag

An experimental program was conducted at Virginia Polytechnic Institute and State University (VPI&SU) (Gonzalez and Easterling 1989). This research program included a series of welded tension member tests. Elastic finite element analyses were also conducted. In this way, an experimental base was established, allowing for further, more refined studies to be performed.

1.2 Literature Survey

Butler and Kulak (1971) evaluated the strength and deformation of inclined fillet welding with various angles to the direction of the applied tension load. The load vs. deformation diagram of each test group indicated ambiguous elastic-plastic properties and an uncertain yield point. Instead of conventional elastic or elastic-perfectly plastic representations, formulations derived from trial-and-error procedures were suggested for describing the relationship between load and deformation, and the relationships between inclined angle and ultimate load and deformation. Another notable conclusion was stated as follows : "Welds placed parallel to the direction of the load have the lowest strength and highest ductility "(Butler and Kulak 1971). The strength of transverse welds is 44% greater than that of longitudinal welds; however, the deformation capacity in longitudinal welds is estimated to be around four times larger than in transverse welds.

Beaulieu and Picard (1987) explained the advantage of studying the behavior of steel connections by the finite element method. Besides the cost, practicability is the primary matter that makes the finite element method an acceptable alternative. As

Beaulieu and Picard pointed out, the experimental approach is still the favorite of scientists because of its honest reflection of reality. However, because of many parameters and the highly complex nature of steel connections, the requirement of an adequate number of specimens was always hard to satisfy. Therefore, finite element analysis became a strong auxiliary tool in developing an ideal model, and modifying the model by means of information obtained from experiments. In the end, some predictions can be made that may be easily checked by further tests. Beaulieu and Picard (1987) also suggested a simplified method to simulate welded and bolted connections with calibrated spring or bar element. The spring constants may be determined from experimental tests on the weld material.

Gonzalez and Easterling (1989) investigated the behavior and strength of various welded members using forty tension tests. Four member types : plates, angles, channels, and structural tees (see Fig. 1-2), and three weld patterns : longitudinal, transverse, and the combination of the former two, were combined systematically in these tests geared towards determining the shear lag coefficient. Besides performing the experimental work, finite element models for each member type were developed. The theoretical stresses derived from finite element analysis appeared to possess fair potential; i.e., improvement could be reached by more effort.

An examination of the AISC specification (Load and Resistance Factor Design 1986) identified several unclear points. These includes: no minimum weld length was defined for different U (shear lag coefficient) values; the value of l (weld length, in.) to be used for angle members unblanced welds is unclear and in spite of their efforts, the attempt to obtain a shear lag coefficient didn't succeed because different welding patterns

of the same member type appeared to disagree with the prediction. Conclusions of relevance to this study include:

1. Shear lag controlled the failure of the plate specimens.
2. For plates connected only by longitudinal welds, connection length was shown to have little influence on the shear lag coefficient.
3. Shear lag did not control the capacity of A36 steel members connected only by transverse fillet welds.
4. Transverse welds enhanced the stress transfer into the connected element of a member.

1.3 Scope of Research

The purpose of this study is to analytically investigate the strength and non-linear behavior of plate tension members which are welded longitudinally along both sides (see Fig. 1-1, welded connection of steel plate) under various load cases and boundary conditions. The objective is to develop a more clear understanding of shear-lag effects in these members and to compare analytical shear lag coefficients with those in the AISC specifications (Load and Resistance Factor Design 1986).

The remaining portion of this thesis is organized as follows :

Chapter 2 discusses the process of FE (Finite Element) model selection. A convergence analysis is performed. This convergence analysis is conducted for both linear and nonlinear cases. A general model is chosen for the use in Chapter 3 and Chapter 6.

Chapter 3 focuses on the nonlinear finite element analysis of the general model. The relationship of load vs. displacement is investigated and presented. Strain responses at different plate positions are calculated. These theoretical results are compared with experimental findings. Experimental data is obtained from the previous study (Gonzalez and Easterling 1989).

Chapters 4 and 5 both focus on practical problems. Chapter 4 deals with eccentric load conditions. Three possible cases are investigated. For each one, an independent eccentricity caused by special arrangements of loads is given. The load vs. displacement response and the change of strain distribution are discussed.

In Chapter 5, two notched plate cases are investigated. These notches are assumed to be caused by improper welding.

Chapter 6 discusses the determination of shear lag coefficient by case study. Each case only differs from the other in weld length. Ultimate loads for each case are calculated and shear lag coefficients are determined.

Chapter 7 concludes the research. Some suggestions for future studies are provided.

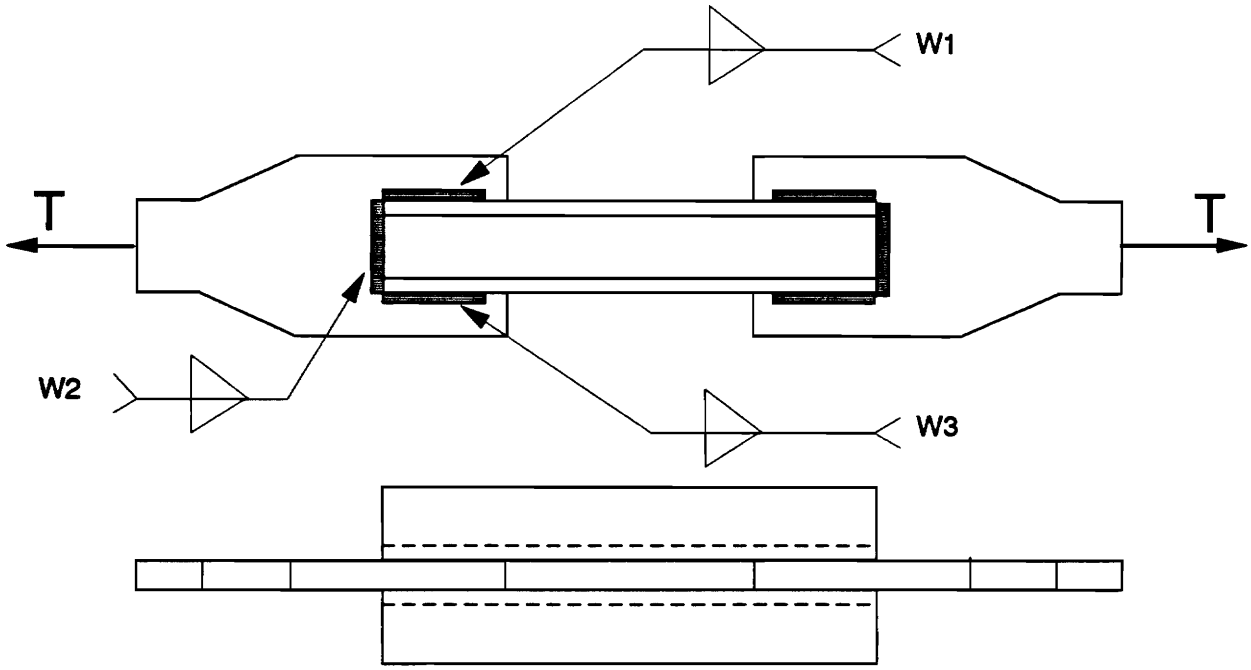

Channel Test Specimen Schemata

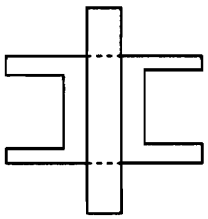

Channels

Similar Specimen Schemata for Other Cross Section

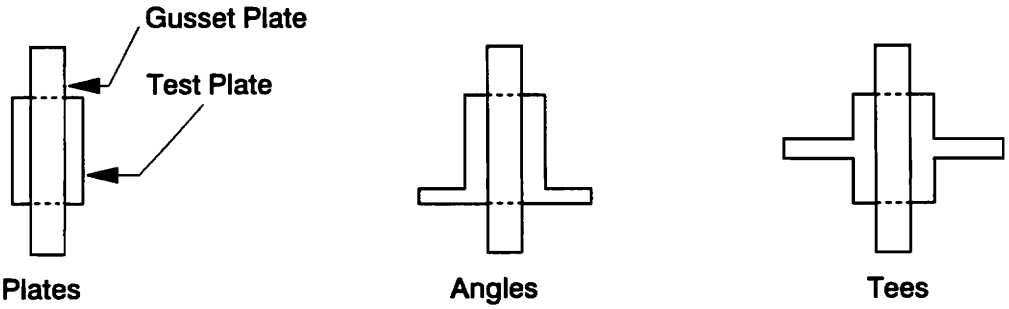

Figure 1-2 Four Member Types of Experimental Test

Chapter 2 Finite Element Model Study

2.1 General

Given that this research concentrates on plate aspects, FE plate meshes from the previous study (Gonzalez and Easterling 1989) serve as an aid in determining the most appropriate FE mesh. Two types of specimens were analyzed in the previous study: (1) plates with longitudinal welds (P-L series) and (2) plates with both longitudinal and transverse welds (P-B series). The following discussion will focus on the P-L type only. A schematic of a typical test specimen in the P-L series is shown in Fig. 2-1, and a photograph of specimen P-L2-2 is shown in Fig. 2-2.

The test plate is arranged to be 6 inches long on the gusset plate, while the welding connection is 5 inches long. This one additional inch of leeway serves to constrain the rotation ϕ_X (the deformation toward Z direction), which may occur to the unwelded part of the test plate.

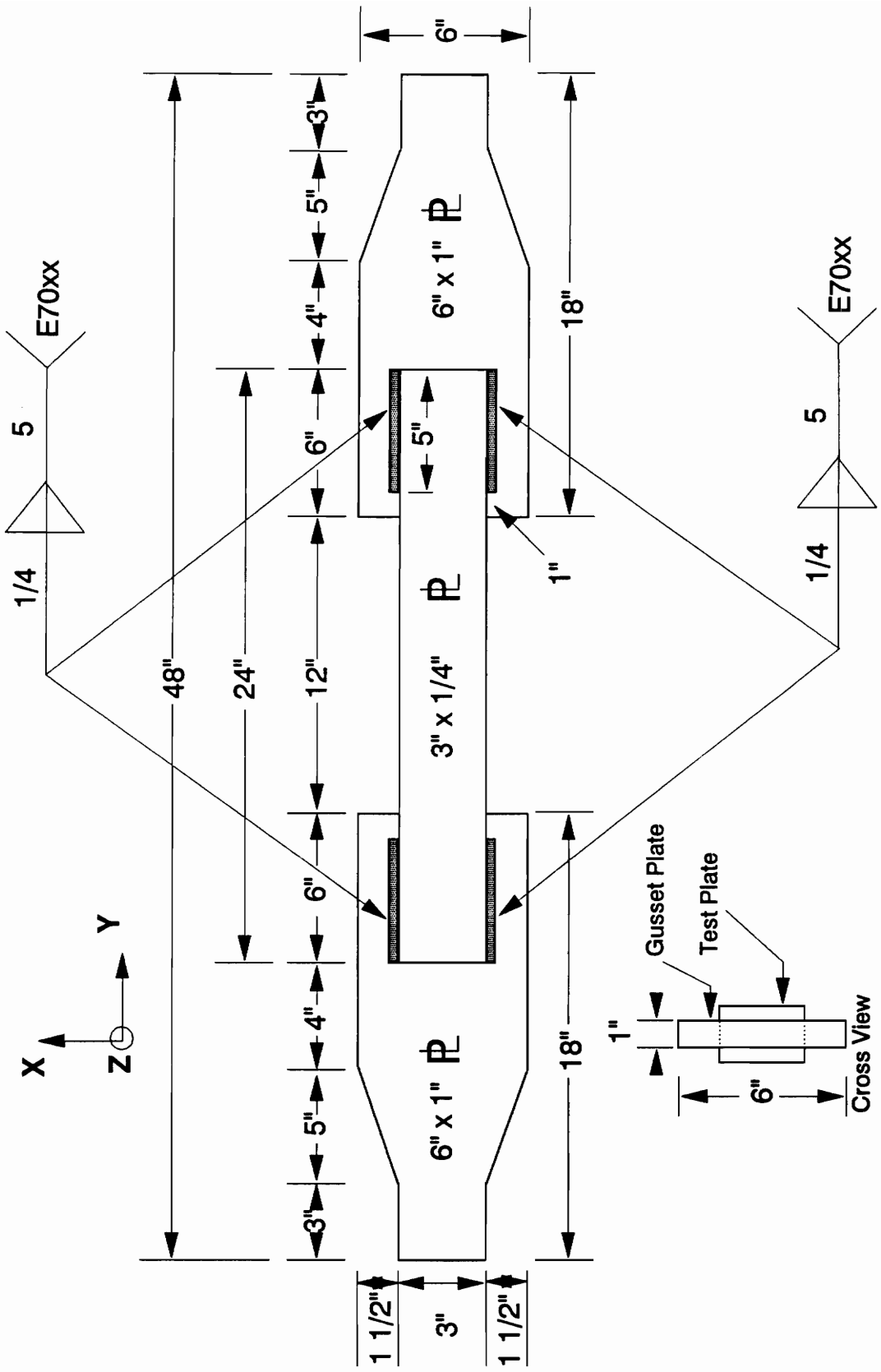

Figure 2-1. Plate Test Specimen Schematic (Gonzalez and Easterling 1989)

Figure 2-2 Experimental Arrangement for P-L2-2 Specimen

Because of symmetry, only one-fourth of the test specimen was modeled(see the crosshatched part of Fig 2-3). However, half of the test plate will be shown for the sake of clarity in illustrating various FE meshes.

2.2 Description of FE Model

In the class of P-L series plates (see p.9), a plate named P-L2-2 was chosen for convergence examination. The reasons for this choice are three-fold. First, it has the desired welding length and arrangement of gages. Second, a detailed strain record is available. Third, it performs better than other plates in the P-L series, where performance means a smaller slip of specimen and a slighter eccentric tension load. A general purpose finite element program (ABAQUS) was used for all analyses in this study.

2.2.1 Dimensions and Material Properities

The geometric and material properties of this plate are as follows:

- Length = 12";
- Cross section = 3" × 0.259";
- Modulus of Elasticity = 29×10^3 ksi;
- Proportional Limit = 55 ksi;

- Elastic-Plastic Material Law is given in Fig. 2-4. The material law was measured in a coupon test performed by Gonzalez but unpublished. This data is transferred into ABAQUS by means of the functions *ELASTIC and *PLASTIC.

2.2.2 Boundary Conditions

The boundary conditions of the FE model are introduced in this section. The command and function cards of ABAQUS, which are utilized for boundary conditions in the study, are mentioned as well.

The function XSYMM of *BOUNDARY is used in modeling of the one-fourth of the plate, ensuring that no transverse displacement and no bending or torsion are allowed along the entire longitudinal midline, which is parallel to the Y axis. Also, the transverse midline (horizontal to the X axis) of the test plate is assumed to remain straight, horizontal, and continuous during tension loading. Accordingly, the *EQUATION command is used to ensure that every node on that line realizes the same displacement.

The welds are simulated by linear spring groups. Each spring group contains two springs for simulating the X and Y axis mechanical responses of welding, illustrated in Fig 2-5. The siffnesses of these two springs are equal. A detailed discussion of the springs is found in section 2.4.

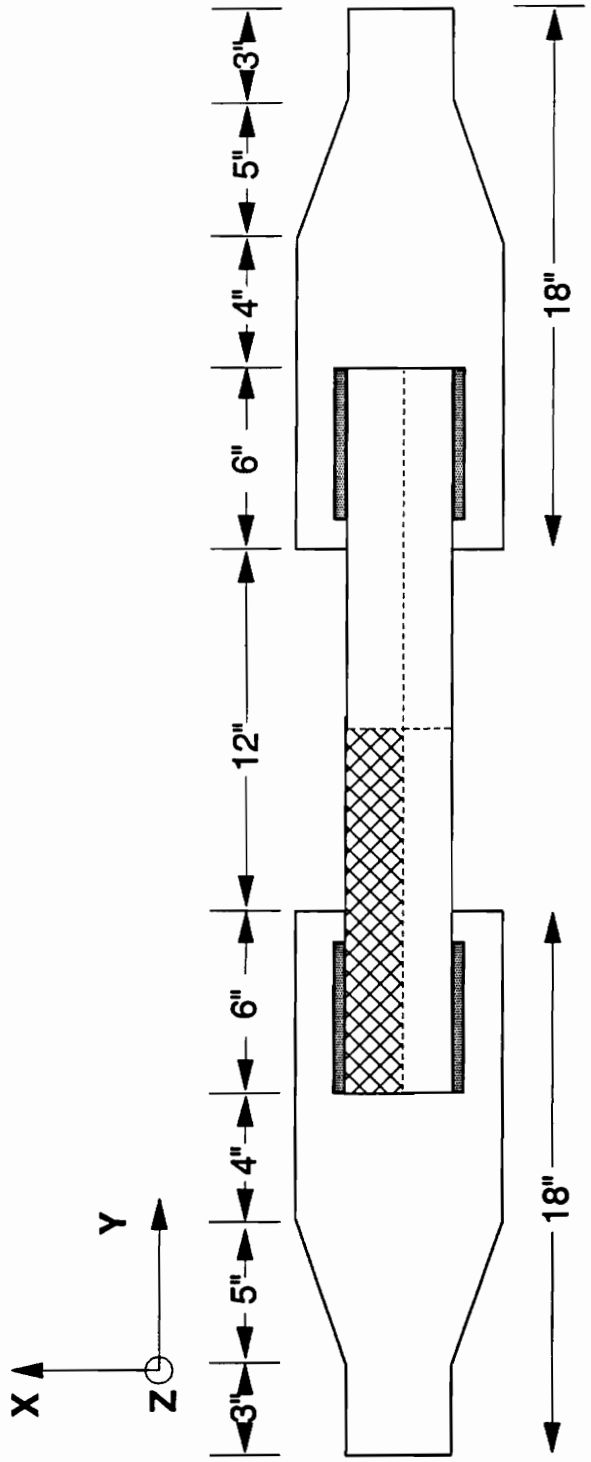

Figure 2-3. Portion of Test Plate Used in FE Modeling

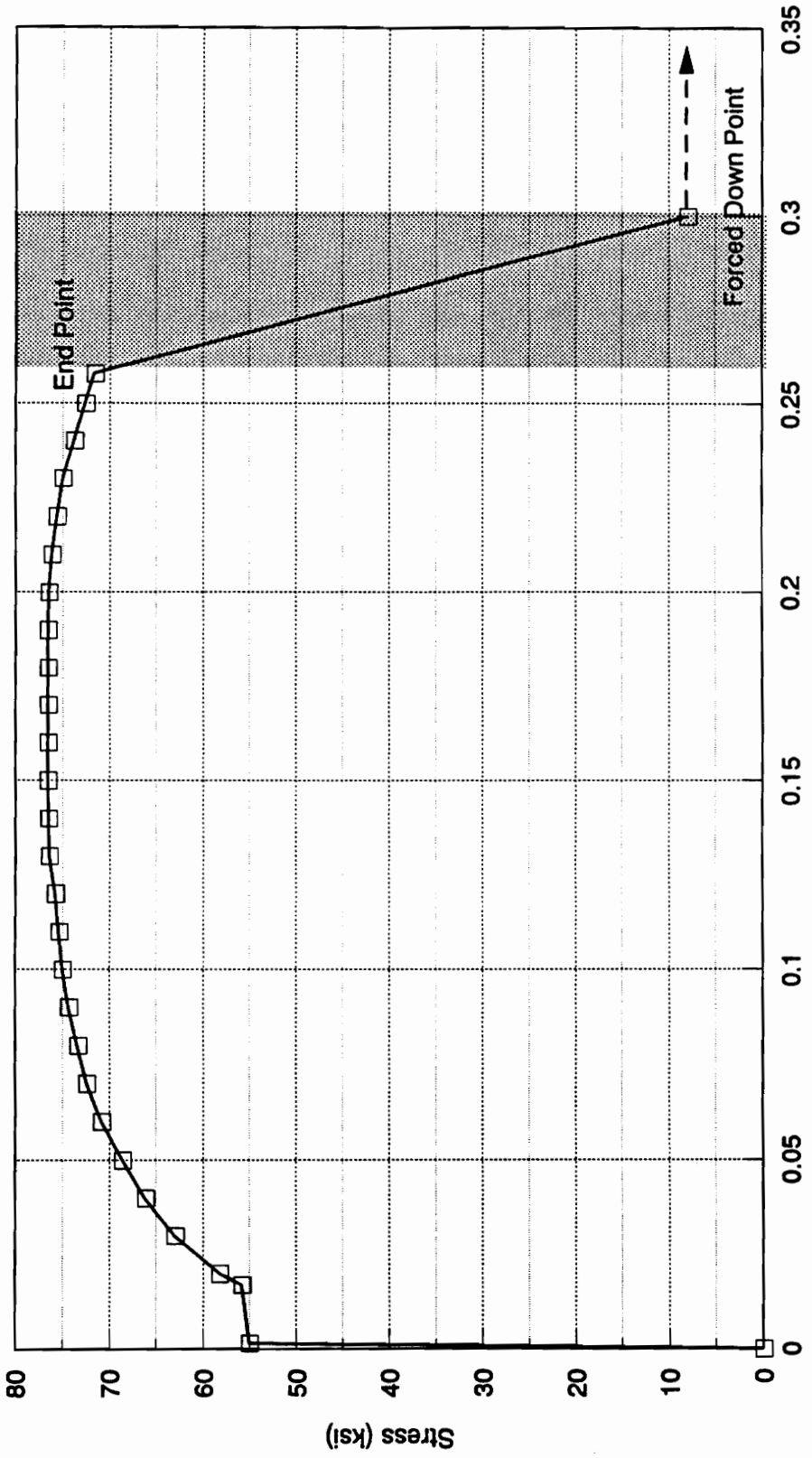

Figure 2-4 Input Material Law for P-L2-2

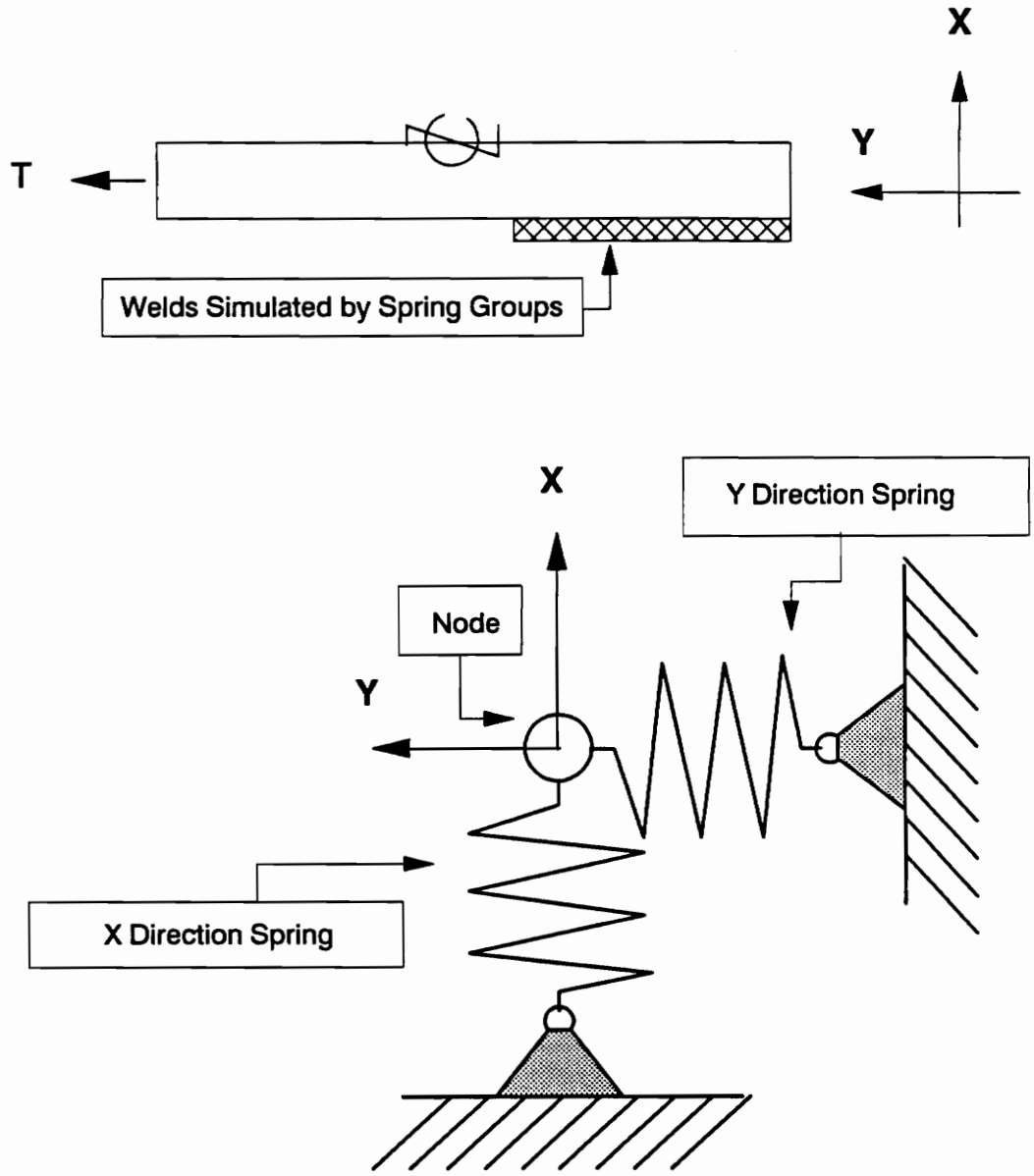

Figure 2-5 Illustration of Spring Group

Besides invoking the XSYMM function and specifying the spring characteristics, no other restraints on the X direction are made. Thus, the part of the edge between the end of the spring groups and the transverse midline is free of restraint.

2.3 Analysis--Methods and Procedures

This study consists of linear and nonlinear analyses. The nonlinear analyses includes material nonlinearity for the steel member, but not for the welds. The nonlinear analysis is used to trace the equilibrium path until the FE calculation is ended by the input limitations. These limitations are set by the PTOL, which is a static-analysis parameter whose value is the basic tolerance measure for solution of the equilibrium equations at each increment. Before the convergent analysis starting, an investigation for determining the value of PTOL was conducted by the FE model of plate P-L2-2. In this investigation, the load versus displacement relationships of different PTOL values were compared. The outcome of that PTOL is equal to 0.1 was found to have the appropriate accuracy and efficiency; therefore 0.1 was used. Once the equilibrium solution is not achieved under the limitation anyhow, the FE analysis is ended.

Two analytical methods provided by ABAQUS are used in this study, the modified Newton-Raphson method and the modified Riks-Wempner method. The load range is from 0 to 30 kips for the linear analysis. Beyond the 30 kips, the stress value in the vicinity of the critical section is greater than the propotional limit (see Appendix A).The yield stress of the plate material is 55 ksi and the corresponging strain is 0.0019 in/in, using 29,000 ksi as the modulus of elasticity. In this part, the nonlinear study is executed and the

modified Riks-Wempner method is used to trace the equilibrium path beyond the proportional limit point.

Once the Riks-Wempner method has been chosen, the current local load magnitude is given by:

$$P_{total} = P_0 + \lambda(P_{ref} - P_0),$$

where

P_{total} = the current magnitude for the load component;

P_0 = the magnitude of the load component at the start of the step;

P_{ref} = the magnitude of the load component as defined in the data for the step;

λ = the load proportionality factor, which is determined by ABAQUS.

If the command *RESTART is not used, this definition becomes simplified as follows:

$P_{total} = \lambda P_{ref}$, because $P_0 = 0$ for the first calculation.

When the Riks-Wempner method is used in nonlinear analysis, the load increment is commonly defined by automatic incrementation. As such, the load values cannot be fixed by the user. Therefore, in this study, the strain and displacement responses of certain applied loads are derived by interpolation. A duplicate of the ABAQUS program is given in Appendix B.

2.4 Investigation of Springs

In modeling the welds, spring groups were employed to simulate welding characteristics. According to the definition of plate shear lag problems, only plate crack failure governs the plate tension strength.

Since no welding failure was reported in the shear lag experimental tests, and because a better spring model is not yet available, the springs in the theoretical analysis are assumed to follow Hooke's law in all instances. The spring stiffness 470 k/in is chosen from the previous study (Gonzalez and Easterling 1989). This value only applies to the case when the number of spring groups is 11. When the number of spring groups changes to 21, the new spring stiffness is calculated as following because the total stiffness is supposed to maintain a constant:

$$470 \times \frac{11}{21} = 246.19 \text{ k/in.}$$

In order to arrange springs for the FE model properly, a spring reactive force distribution vs. spring group position was formulated by analyzing the FE model for plate P-L2-2. The results of this analysis are shown in Figs. 2-6, 2-7, and 2-8. Figure 2-6 shows that the reactive force distribution of the X direction springs changes in no readably discernible way when compared with the changes of Y direction springs (refer to Fig. 2-5 for X and Y orientation); nevertheless, due to the sake of scale, the changes between different load stages are still clear. The maximum reactive force parallel to the X axis always occurs at the initial spring. Figure 2-7 demonstrates that the reactive force of the Y

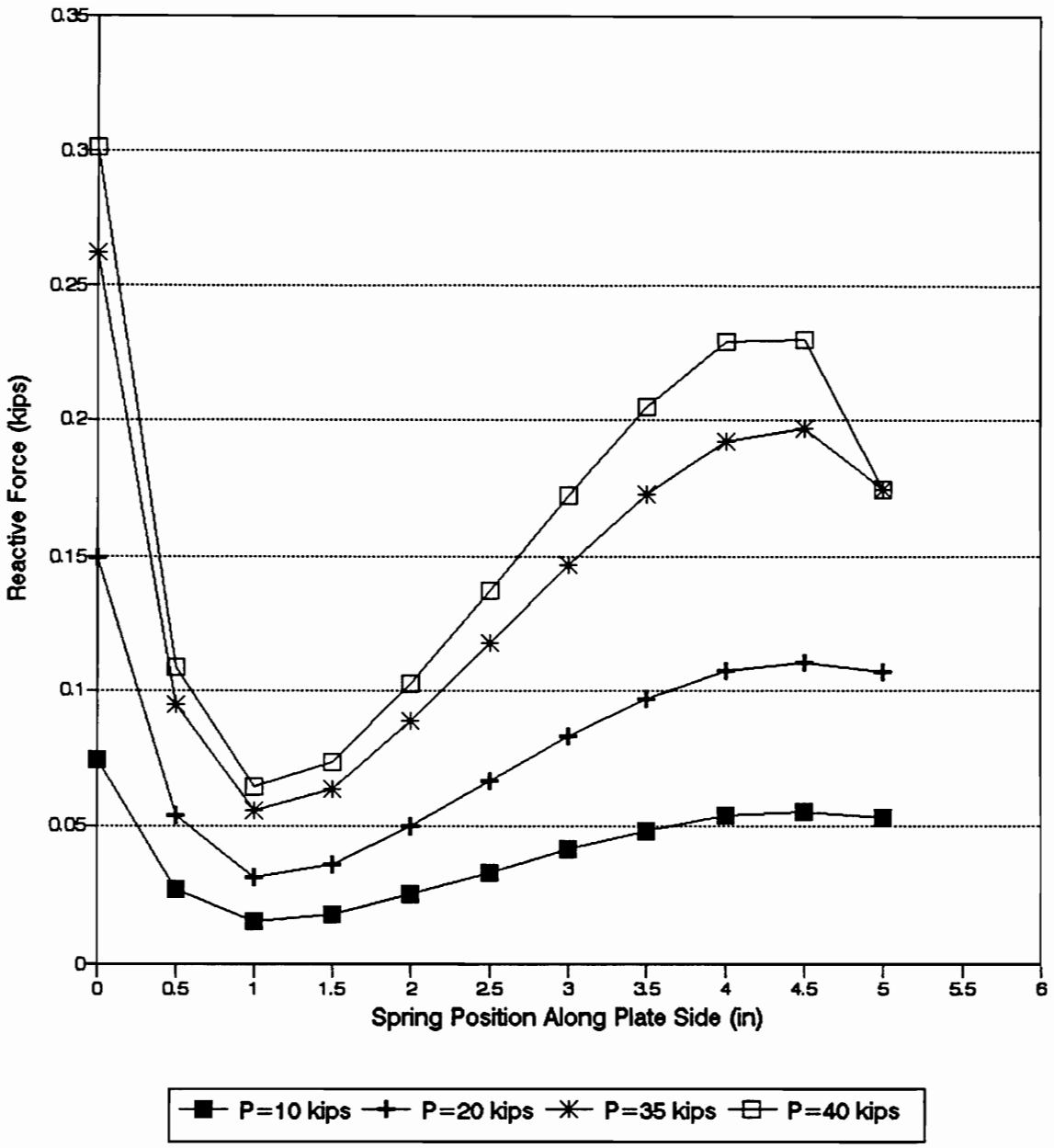

Figure 2-6 Reactive Force of X-Direction Springs Along Longitudinal Side of P-L2-2 Model

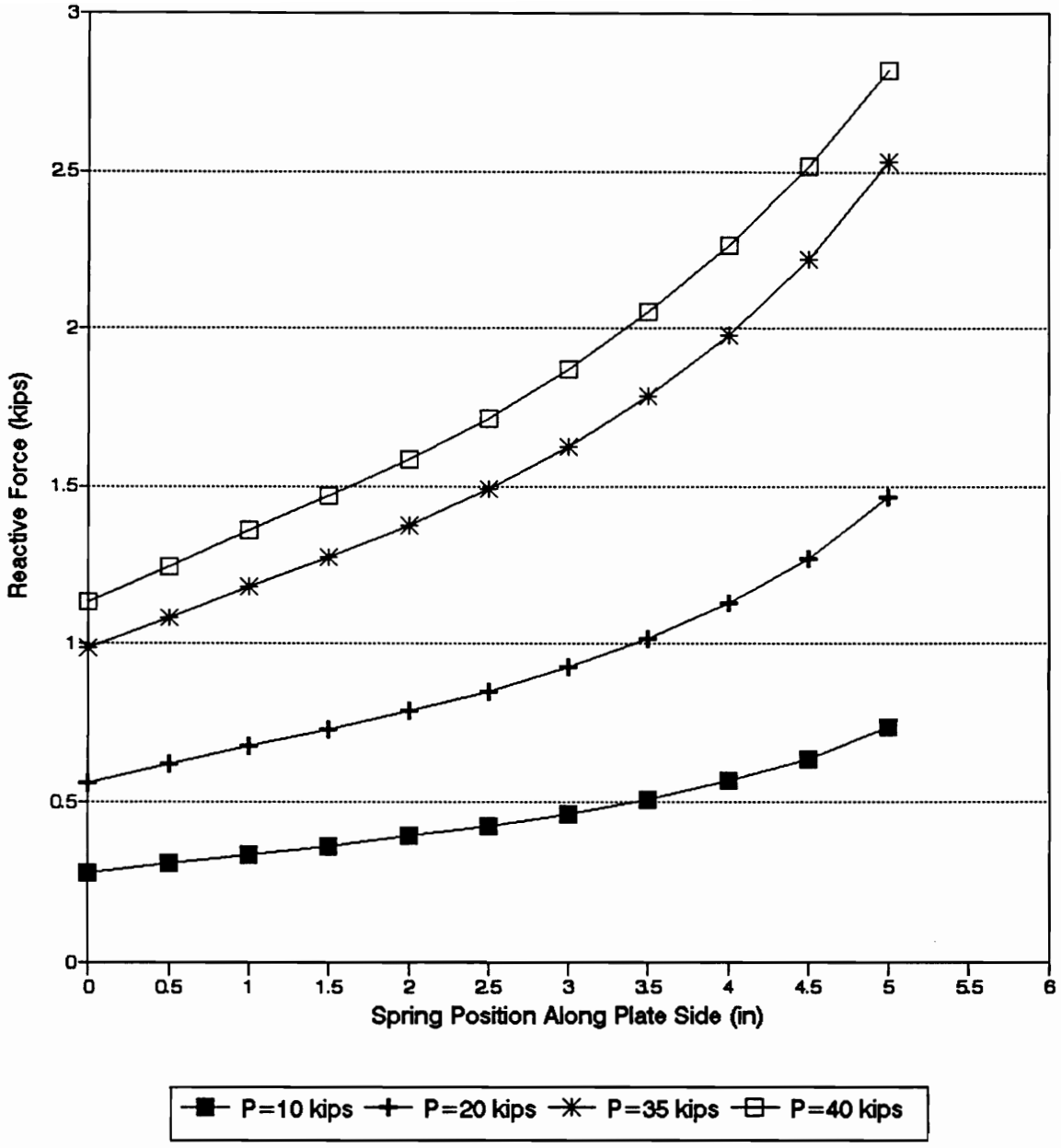

Figure 2-7 Reactive Force of Y-Direction Springs Along Longitudinal Side of P-L2-2 Model

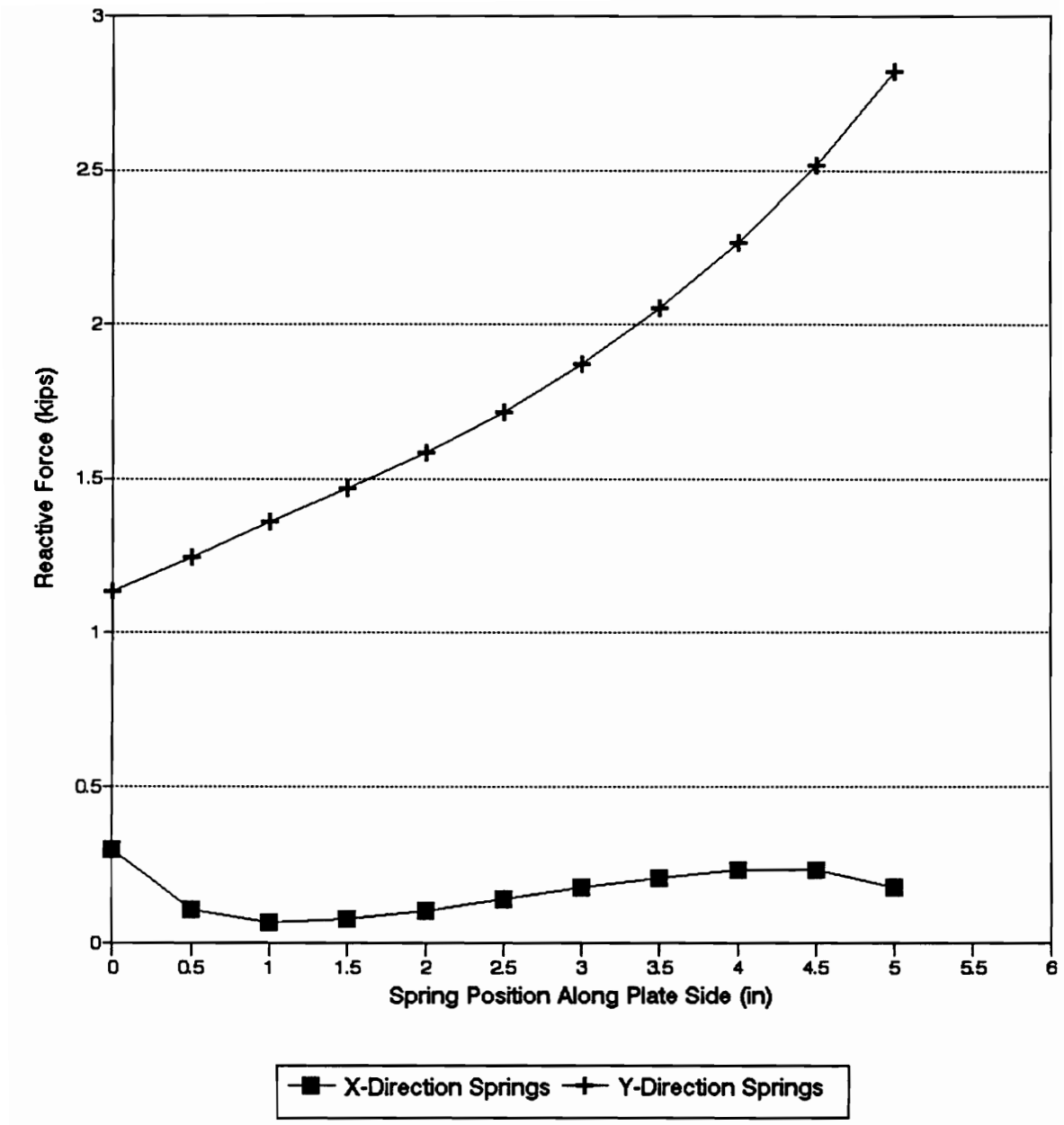

Figure 2-8 Force Comparison Between X-Direction and Y-Direction Springs Under 40 kips Tension Load

direction springs gradually increases from the initial spring to the end, according to a second or higher order function relationship. In addition, the force increment of the end spring is much larger than that of the other springs as the applied load increases. In Fig. 2-8, the force curve of the Y direction springs is significant compared with the one of the X direction springs. To determine a sufficiently accurate model for use in further studies, convergence tests were performed on several FE meshes.

2.5 Convergence Investigation

2.5.1 Methods of Investigation

To construct the most accurate FE model for subsequent analysis, the 8-node biquadratic element type, CPS8, is chosen from the plane stress element family of ABAQUS and will be used in the convergence investigation.

The "h-convergence" method which involves identical elements (CPS8) taken in various meshes was used to perform the convergence investigation. In this study, trials will be performed with five different amounts of elements: 26, 78, 144, 432 , and 576, henceforth referred to as the A mesh, B mesh, C mesh, D mesh, and E mesh, respectively (see Table 2-1, Figs. 2-9 ~ 2-13). These numbers are chosen on the basis of their utility, given the specific experimental arrangement of the specimen's reported previously

(Gonzalez and Easterling 1989), and the general principles of FE convergence analysis; for instance, the sequence of regular mesh refinements requires that the finest mesh contain all previous meshes.

Table 2-1 Description of Various FE Meshes

Mesh Name	A	B	C	D	E
No. of Elements Contained	26	78	144	432	576
Element Size (in × in)	1.5 × 1 1.5 × 0.5	0.5 × 1 0.5 × 0.5	0.5 × 0.5	0.25 × 0.25 0.25 × 0.5	0.25 × 0.25

2.5.2 Procedure of Convergence Investigation

Increasing load stages from 10 to 40 kips are applied on the meshes with CPS8 element type by the modified Newton-Raphson method. Because the experimental strain values on gages 1 to 8 were recorded in the previous study, the FE studies focus mainly on the positions corresponding to gages 1 to 8. These positions are named as G1,G2,G3,G4,G5,G6,G7,and G8 and are located by the following table 2-2 and Fig. 2-14.

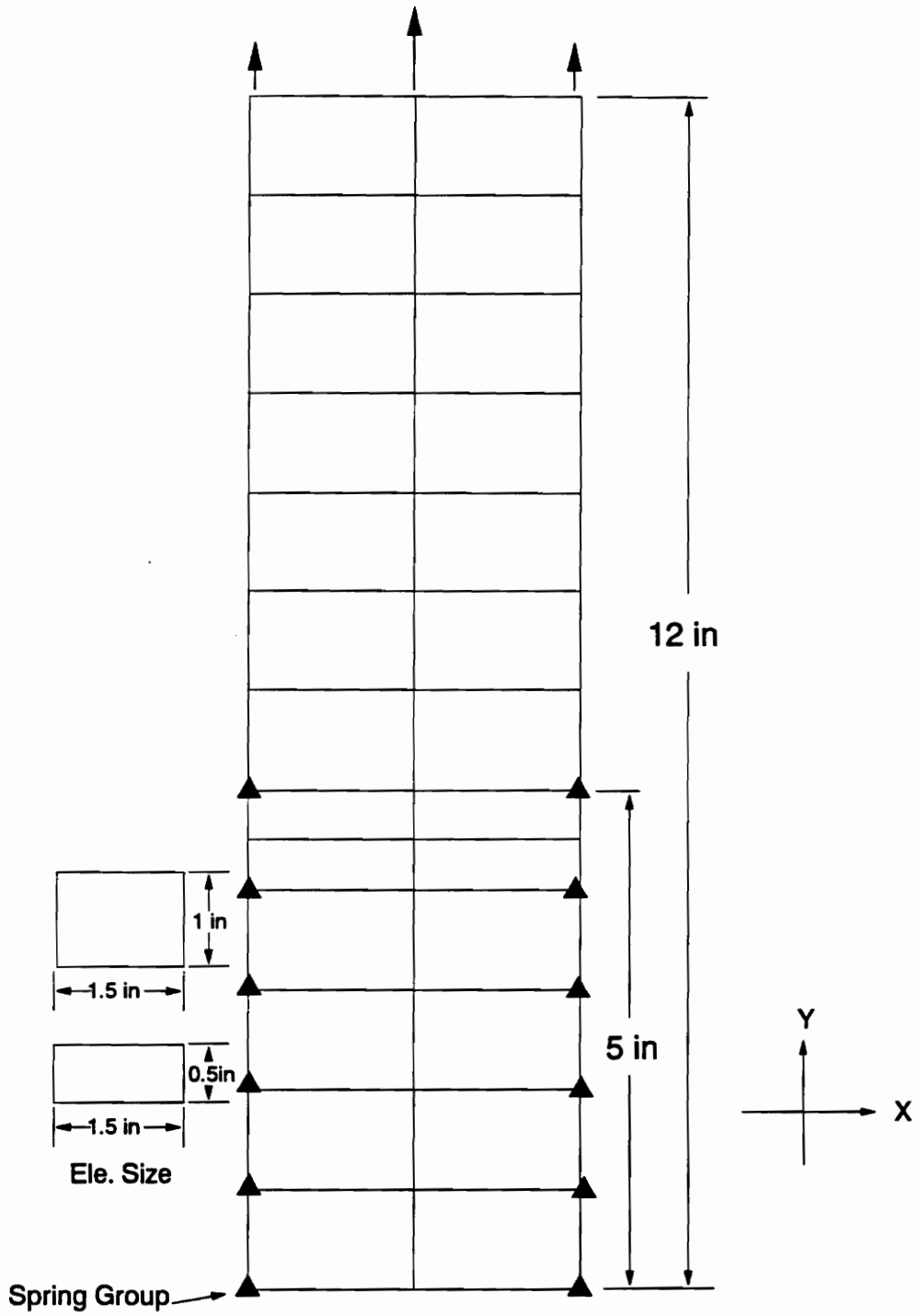

Figure 2-9 Illustration of A Mesh (26-Element Mesh)

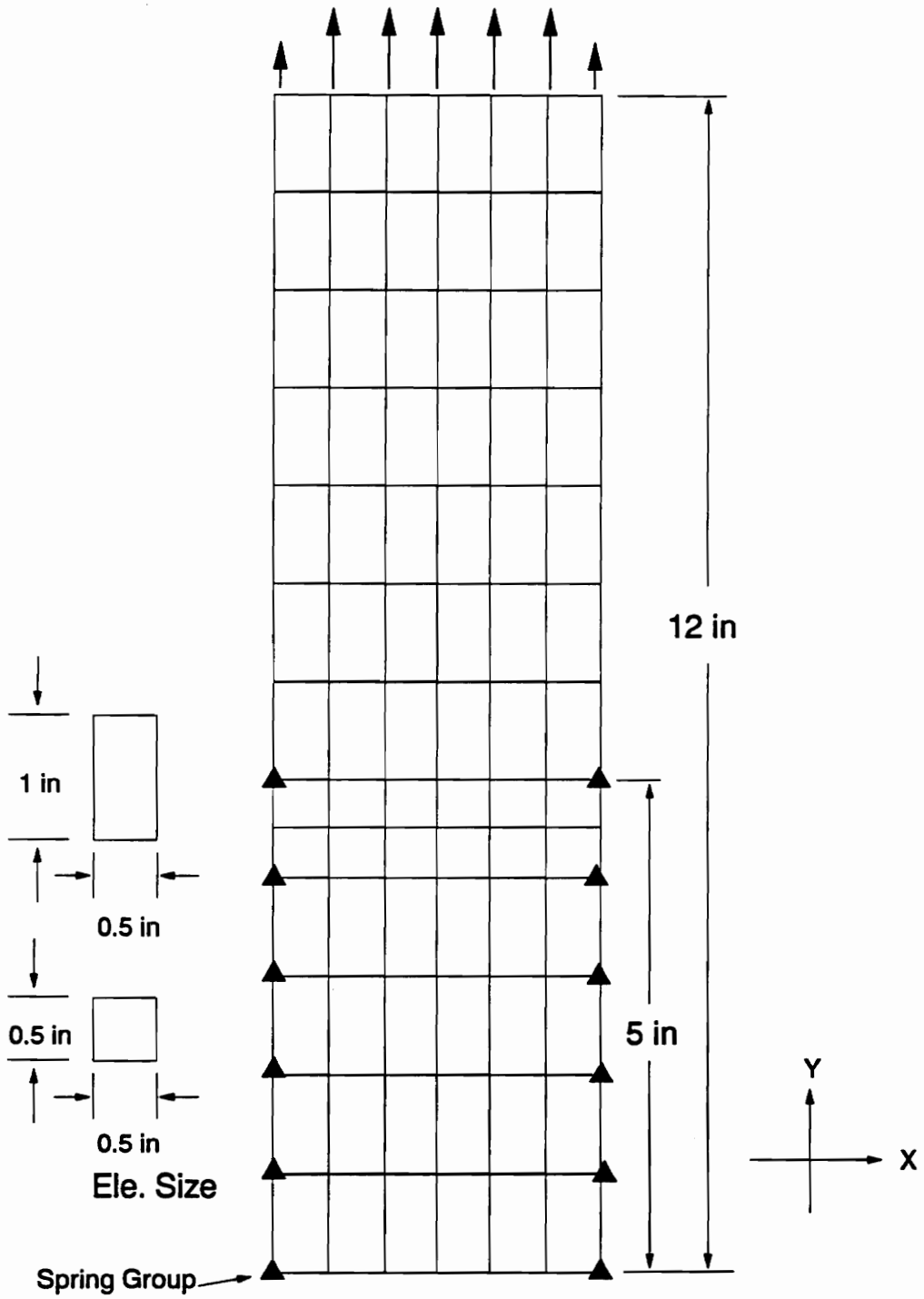

Figure 2-10 Illustration of B Mesh (78-Element Mesh)

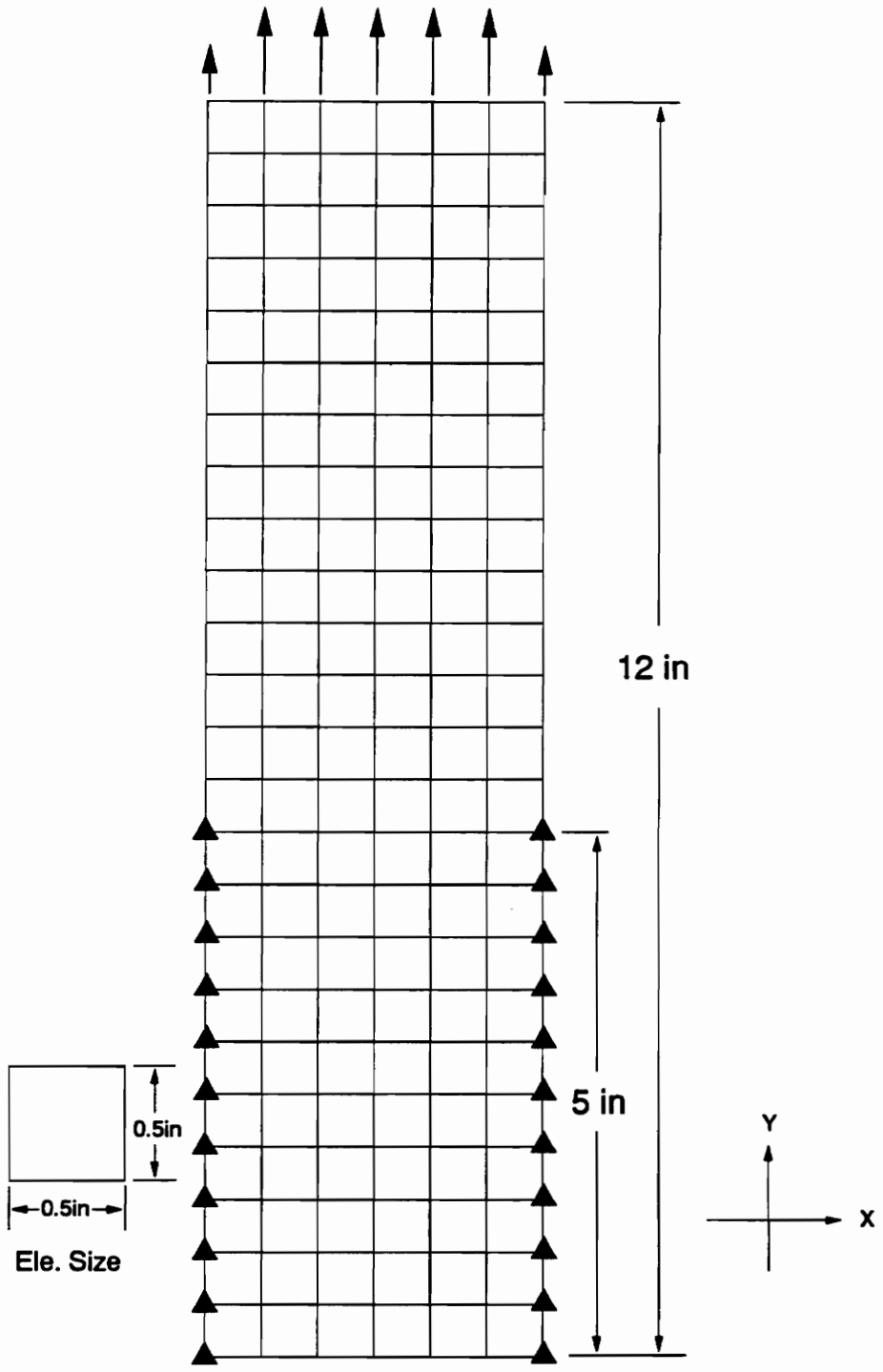

Figure 2-11 Illustration of C Mesh (144-Element Mesh)

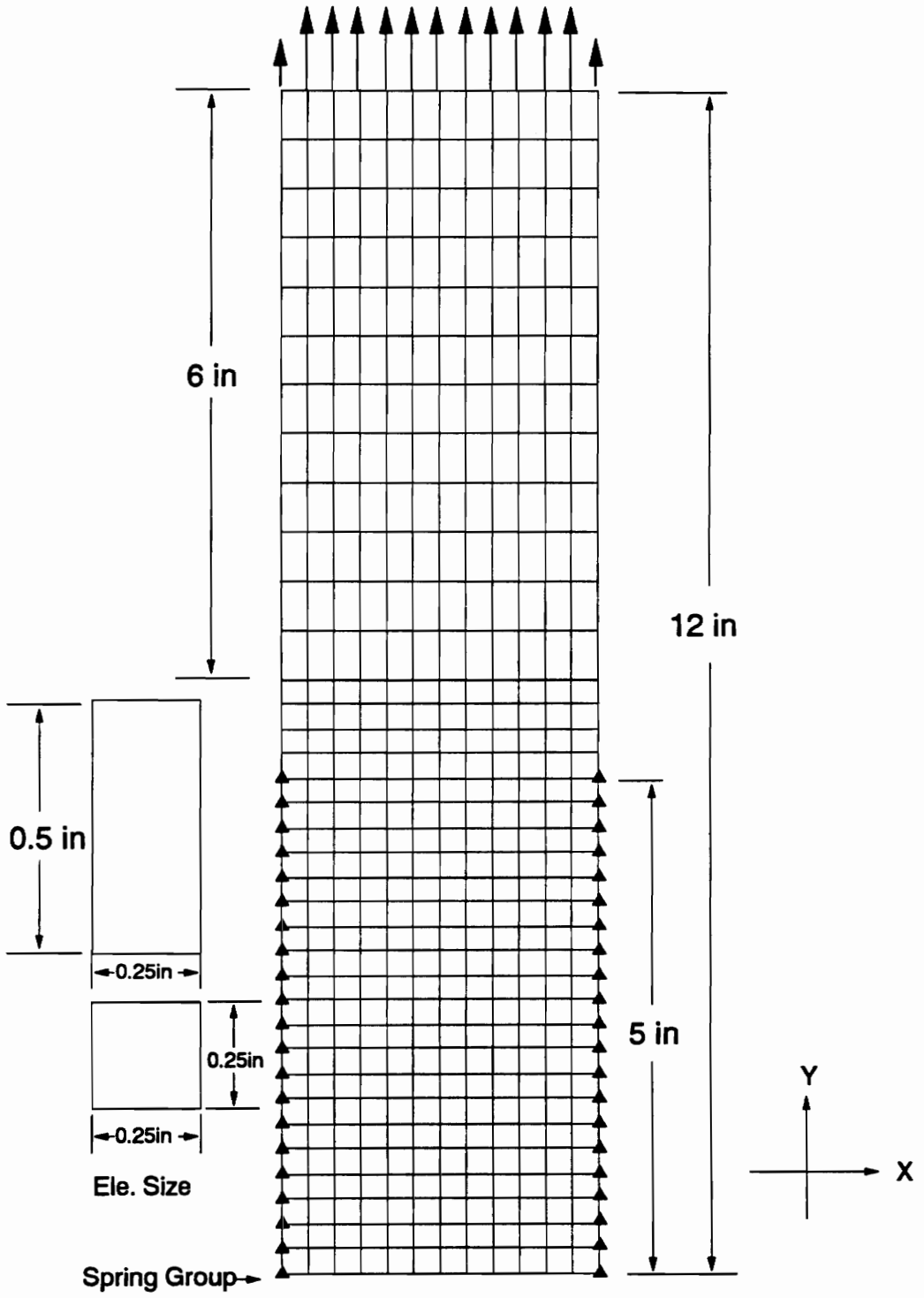

Figure 2-12 Illustration of D Mesh (432-Element Mesh)

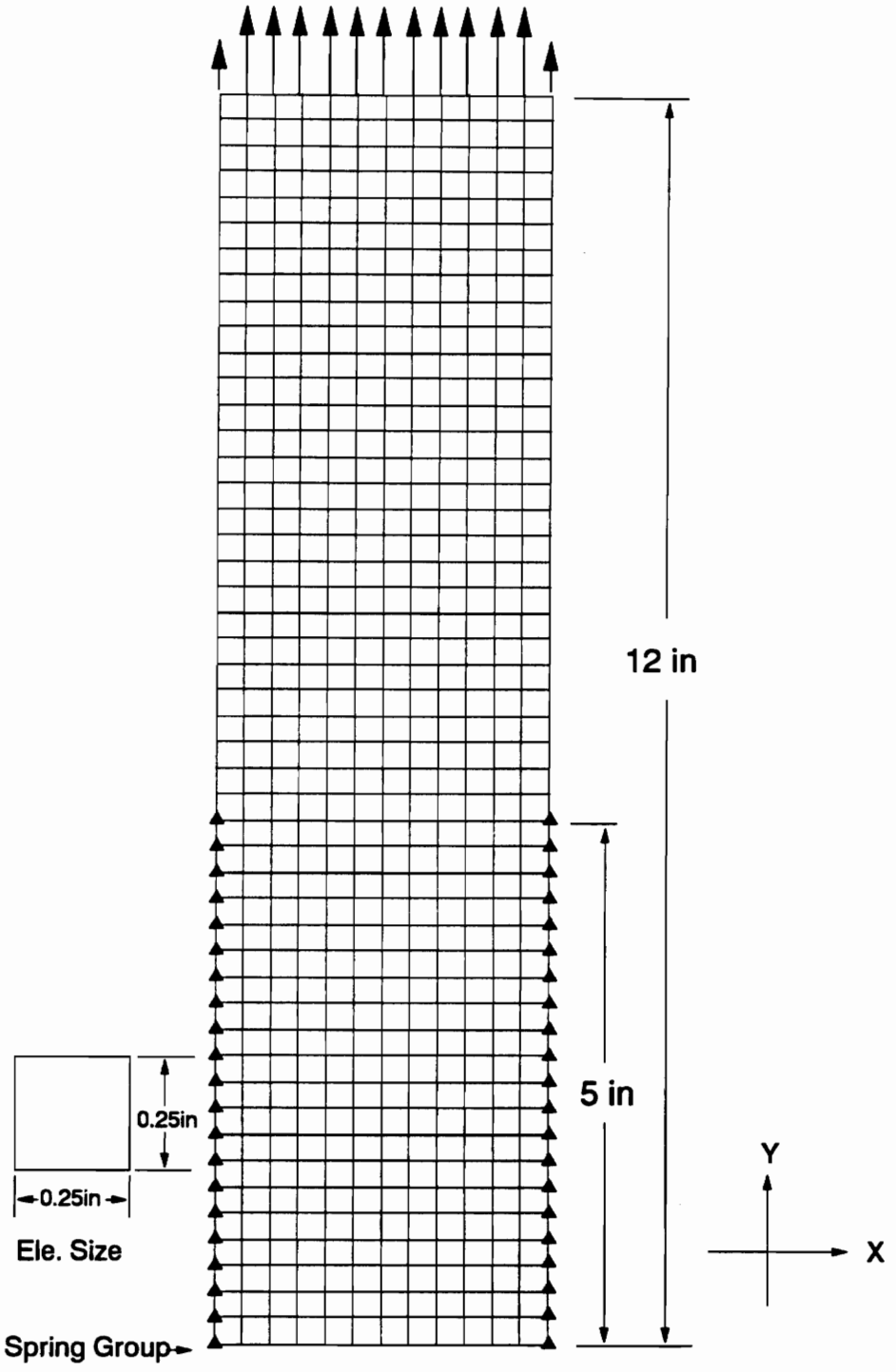

Figure 2-13 Illustration of E Mesh (576-Element Mesh)

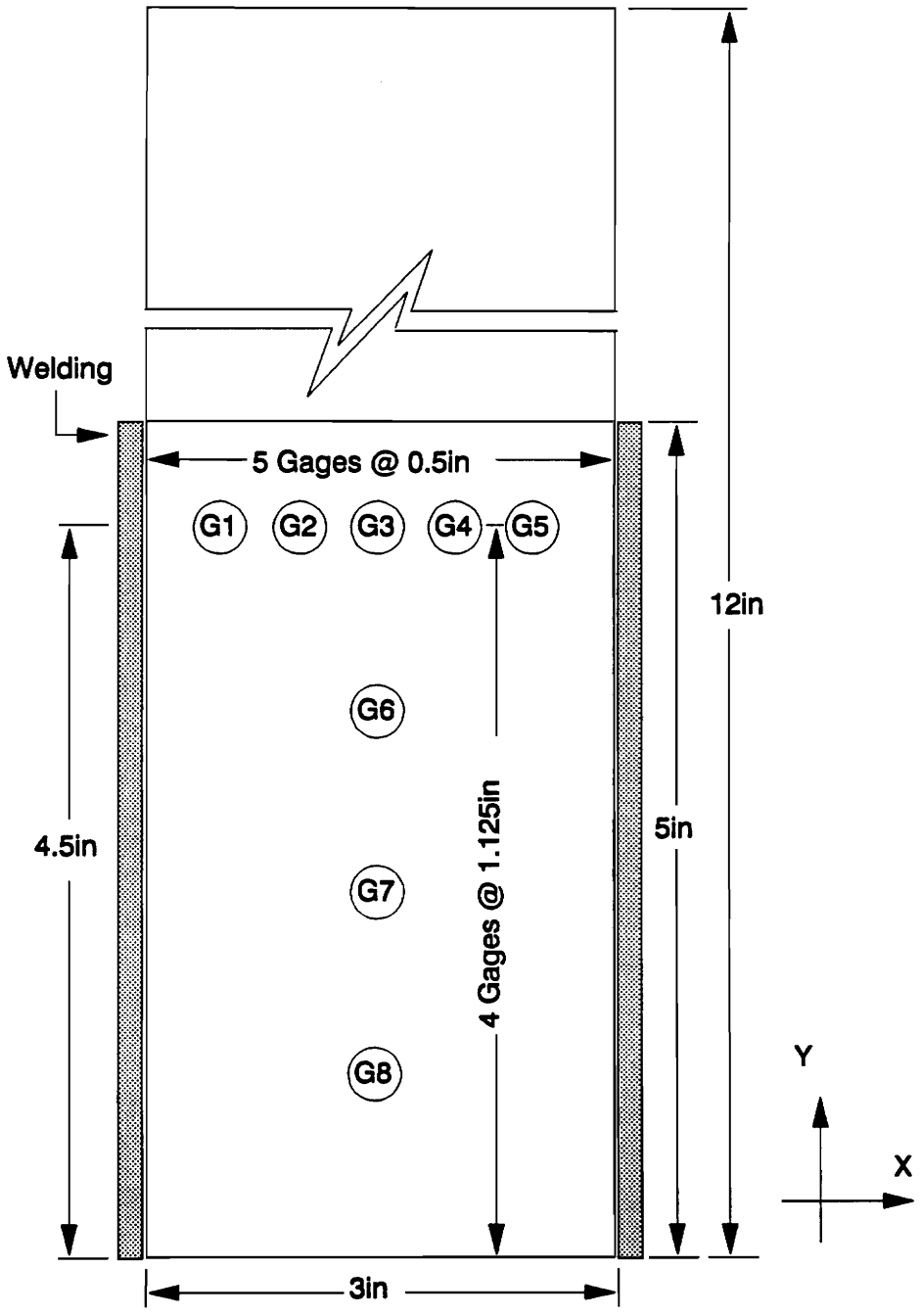

Figure 2-14 Position of Test Gages and Positions of Response Measurements in FE Analysis

Table 2-2 Coordinates of The Gage Positions

Position Symbol	G1	G2	G3	G4	G5	G6	G7	G8
X Coordinates (in)	0.5	1	1.5	2	2.5	1.5	1.5	1.5
Y Coordinates (in)	4.5	4.5	4.5	4.5	4.5	3.375	2.25	1.125

Due to the singular positions, the strain values of G6, G7 and G8 have to be derived by interpolation in meshes A and B. This may result in an incorrect convergence analysis outcome; therefore, convergence investigation is merely conducted on G1 to G5. For positions G1 and G2, strain values of meshes B to E are derived and drawn with a continuous line connecting the data points. For position G3, the A mesh is available so the considered meshes become A to E. Analytically, the strain values of G4 and G5 are not necessary to show because of the symmetry; so only the values of G1 to G3 are investigated. A clear relationship between the measure positions, loads, and various FE meshes is given in Table 2-3. The outcomes of convergence investigation are illustrated in Figs. 2-15~2-17.

Table 2-3 The Relationship Between Various Considerations for Convergence Investigation

Measure Position	G1	G2	G3
Load Investigated (kips)	10,20,30,35,40	10,20,30,35,40	10,20,30,35,40
FE Mesh Used	B,C,D,E	B,C,D,E	A,B,C,D,E

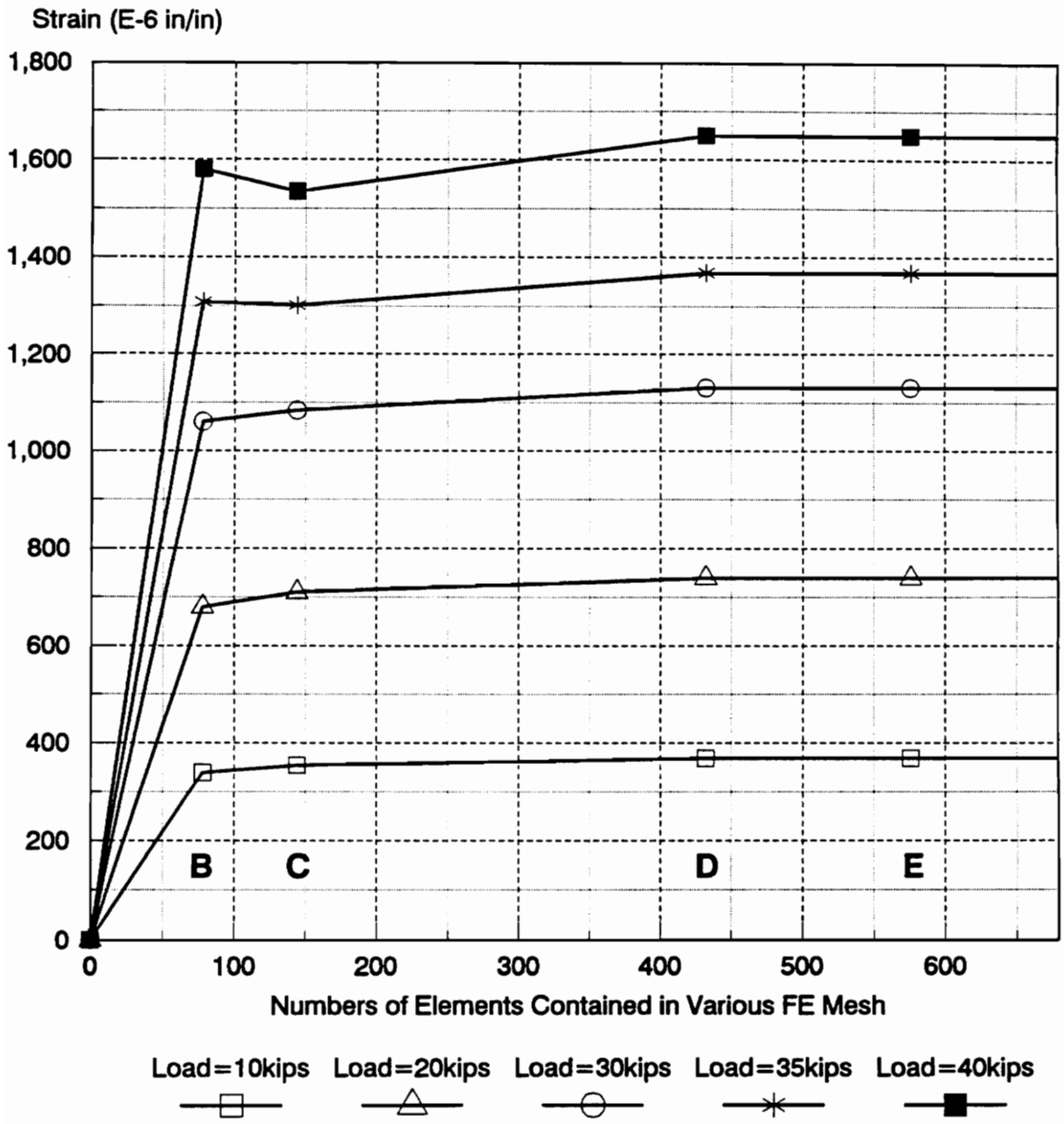

Figure 2-15 Convergence Analysis at Position G1 for Various Element Meshes and Applied Tension Loads

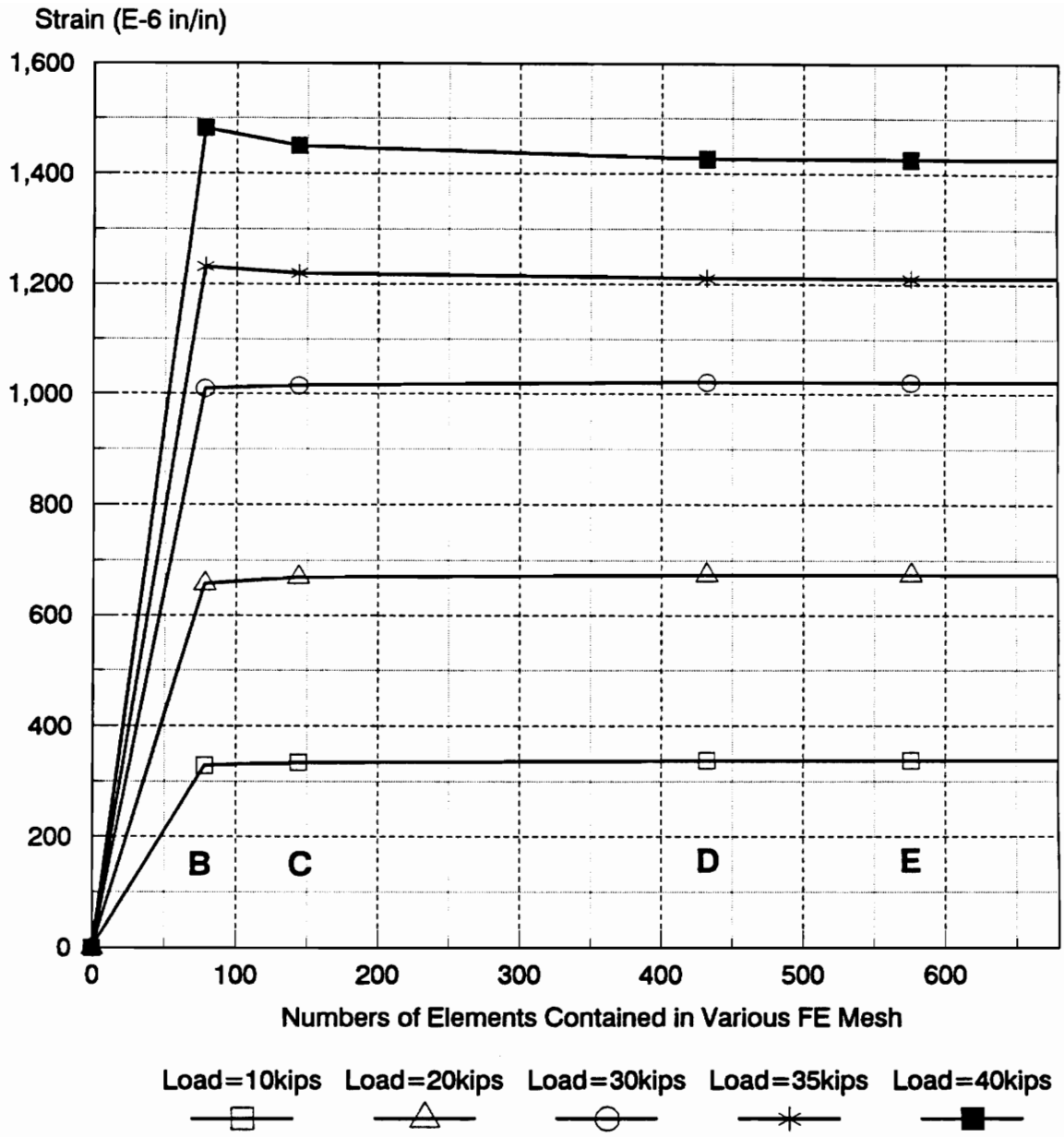

Figure 2-16 Convergence Analysis at Position G2 for Various Element Meshes and Applied Tension Loads

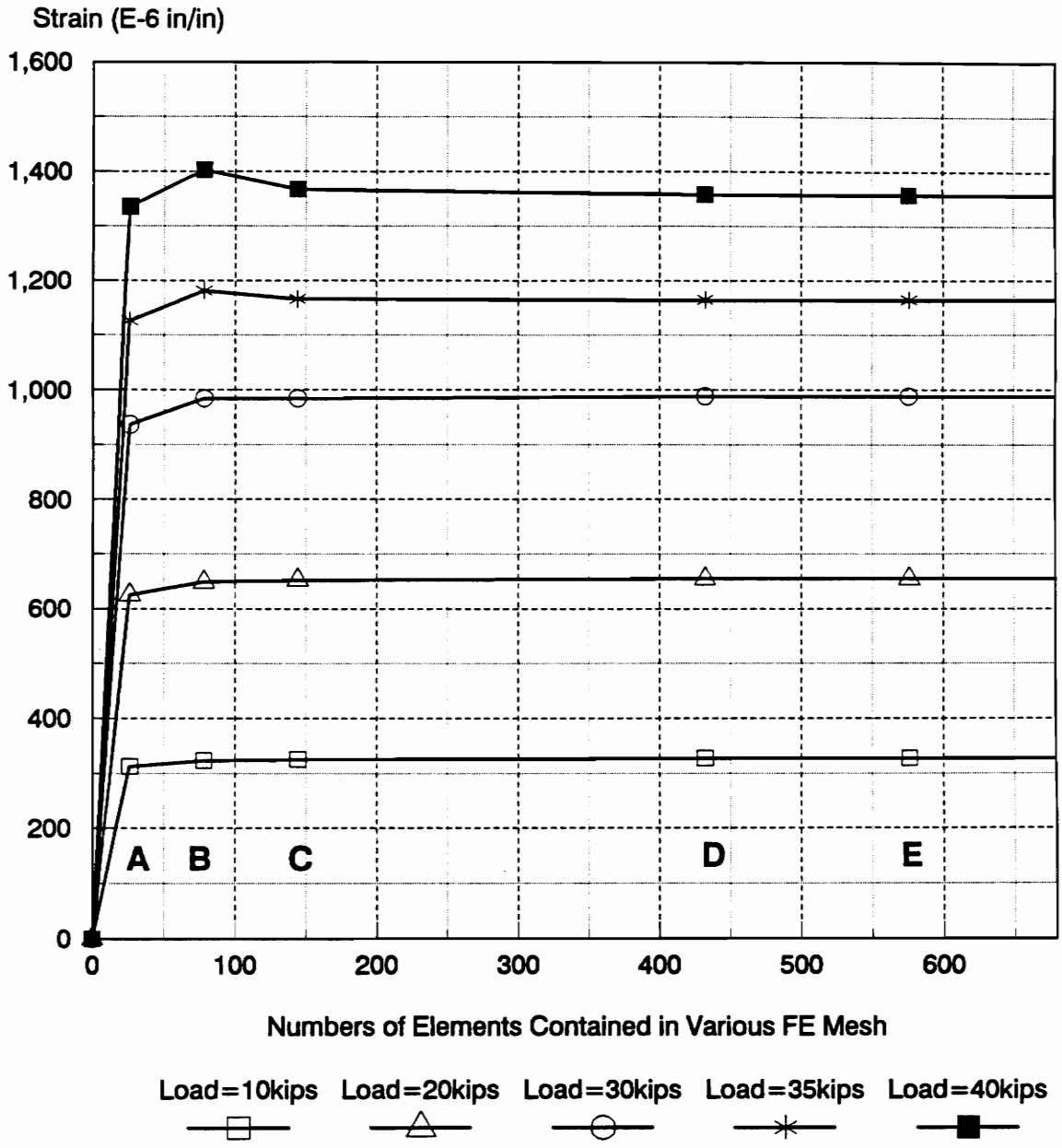

Figure 2-17 Convergence Analysis at Position G3 for Various Element Meshes and Applied Tension Loads

2.6 Determination of Approximate General Model

The FE convergence analysis is complete if the mechanical responses (strain, stress, or displacement) of the chosen nodes are unchanged with additional refinement. If the response values of every refined mesh constitute a monotonically convergent line, the last mesh is considered an approximate mesh. In this study, all three mechanical responses are checked. Due to the similarity, only the outcomes of strain are shown in Figs. 2-15 to 2-17.

Observing these three figures, it is evident that in the linear range (tension load = 10 kips ~ 30 kips) the strain values converge monotonically and rapidly. On the other hand, in the nonlinear range (tension load = 35 kips and 40 kips) the strain value of the B mesh is abnormally larger which causes the convergence to be non-monotonic. This phenomenon is shown clearly in Fig. 2-17. However, a convergence value is still obtained for the E mesh.

Several conclusions may be drawn from the convergence illustrations:

1. For the plate shear lag problems, monotonically convergent values may only be derived in the linear analysis. Non-monotonic convergence is observed for the D and E meshes in the nonlinear range.
2. In the nonlinear part, the more the mesh is refined, the more clearly convergence is evident, which implies that the mesh needs to be highly refined to serve in the nonlinear analysis. In this study, the E mesh is more refined than the other meshes.
3. In shear lag problems, due to the special transmition of loads, the arrangement of elements (includes element size and position of restraints) may influence the

convergence. To perform an accurate analysis, a square refined mesh is recommended for the nonlinear analysis.

4. The 576-element mesh has proven to be the most appropriate one and, as such, is chosen for use in the nonlinear FE analysis discussed in Chapter 3.

Chapter 3 Nonlinear Analysis---General Case

3.1 General

The primary purposes of conducting a nonlinear analysis are: (1) to determine the theoretical ultimate load of P-L2-2 in this chapter; and (2) to calculate the shear lag reduction factor. The determination of the ultimate load is discussed in section 3.3. Upon determining the ultimate load, the reduction factor is obtained in Chapter 6 by comparing the theoretical ultimate load with the ultimate load predicted by the AISC specification (Load and Resistance Factor Design 1986).

The strain distribution contours (postprocessed using IDEAS) provide insight into the observed nonlinear behavior. In this nonlinear analysis, the FE model is 576-element mesh, the most appropriate one as determined in section 2-6.

3.2 Results

The strain values of positions G1 to G3 and G6 to G8 are recorded at every load stage, with data provided in Table 3-1. Most of these load stages are chosen to correspond to the recorded experimental loads; however, as noted above, some values can only be achieved through interpolation. The load vs. displacement diagram of the general model is shown in Fig. 3-1, where the displacement value is measured from the nodes on the transverse neutral line. The strain contours at loads of 20 kips and 54.7 kips (which is the analytical failure load) are given in Figs. 3-2 and 3-3. A detailed local enlargement of the critical section with the applied load of 54.7 kips (same as that of Fig. 3-3) is given in Fig. 3-4. This figure is drawn with the use of a special function "fringe contour," and it expresses a reliable strain distribution, one more in line with empirical findings. All of the strain contours are processed and produced using the program IDEAS.

Table. 3-1.

Finite Element Analysis--Strain Values for Surveying Positions G1-G3 and G6-G8							
Strain Unit = E-6 in/in; Load Unit = kips; Displacement Unit = in.							
Load	G1	G2	G3	G6	G7	G8	Displacement
10	369	338	328	253	152	54	0.0048
20	739	675	655	505	304	108	0.0097
30	1132	1022	989	765	459	163	0.015
35	1368	1211	1165	908	540	192	0.017
40	1651	1427	1358	1072	628	222	0.02
42.84	1803	1572	1488	1181	682	239	0.029
44.9	2047	1659	1575	1251	719	252	0.137
45	2067	1662	1580	1255	721	253	
45.936	2255	1700	1624	1291	739	258	0.1548
49.872	3397	1973	1799	1472	818	282	0.241
50	3487	1977	1805	1479	821	283	
50.64	3934	1995	1836	1513	834	286	0.263
54.7*	22106	19236	18193	1791	944	318	0.43

Underlined Value -- Interpolated Value

*** Largest Load**

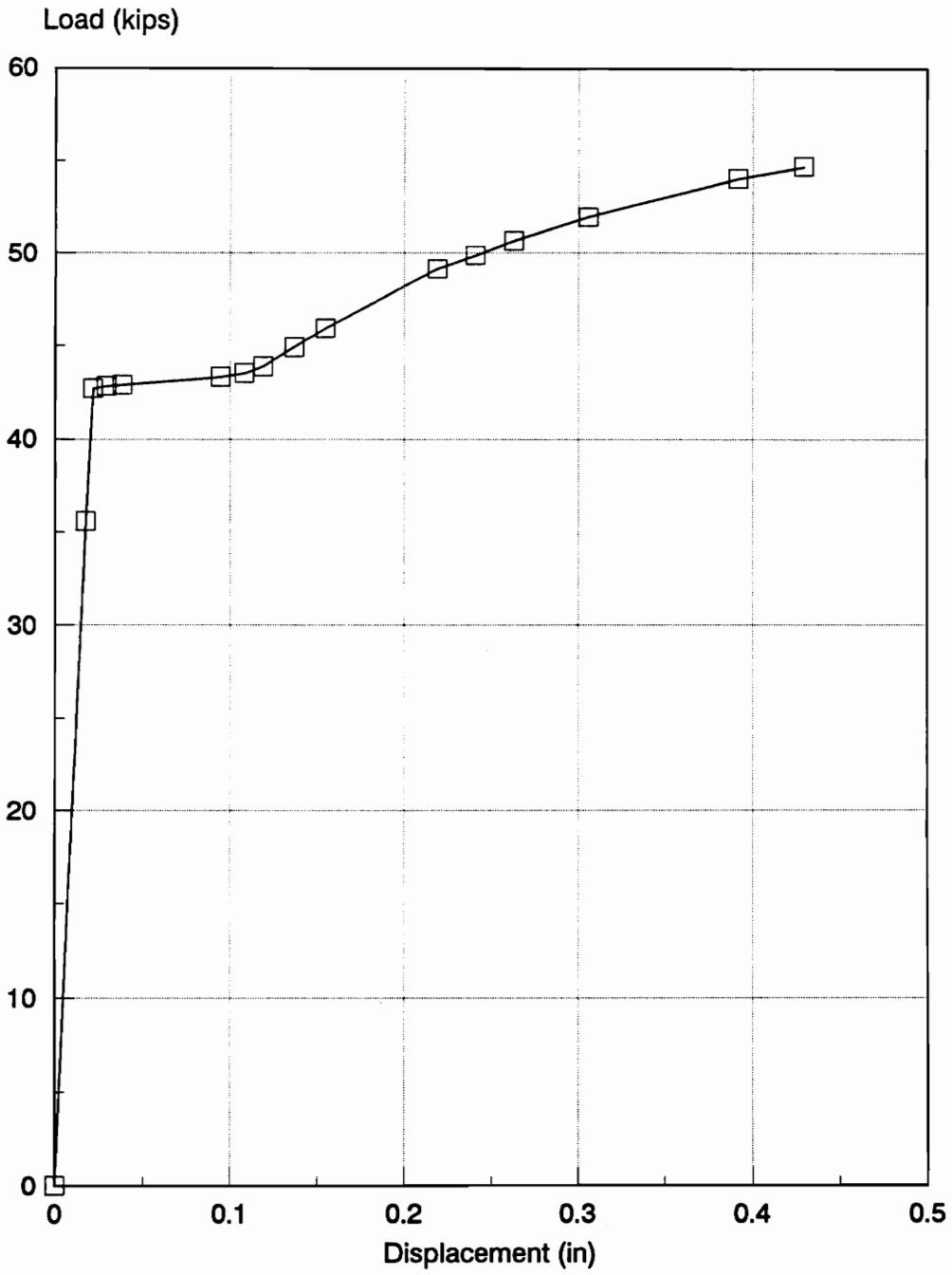

Figure 3-1 Load-Displacement for Analytical Plate General Model

3.3 Observation and Comparison of Results

The strain contours indicate that large strains concentrate at the critical section for both linear and nonlinear analyses (see Fig. 3-2 for linear case and Fig. 3-3 for nonlinear case). The lower areas, near the bottom of the plates, register small strain values in all cases. The maximum strain, for each applied load, is located at the edge, about 0.125 inches above the end of the welding.

While the load-displacement diagram of FE analysis (Fig. 3-1) shows clear strain hardening, the experiment diagram shows sudden crack failure occurring at the top of the increasing curve (see Appendix B). An analytical strain graph for positions G1-G5 (transverse), with a load of 45 kips, is given, with the corresponding experimental data (found in Appendix B), in Fig. 3-5.

The observation and comparison of the theoretical and experimental results indicate the following:

1. The distribution of the strain is slightly asymmetric in the experimental specimen, with the asymmetry varying and switching from one side of the plate to the other as the load increases (see Appendix B, Fig B-2);

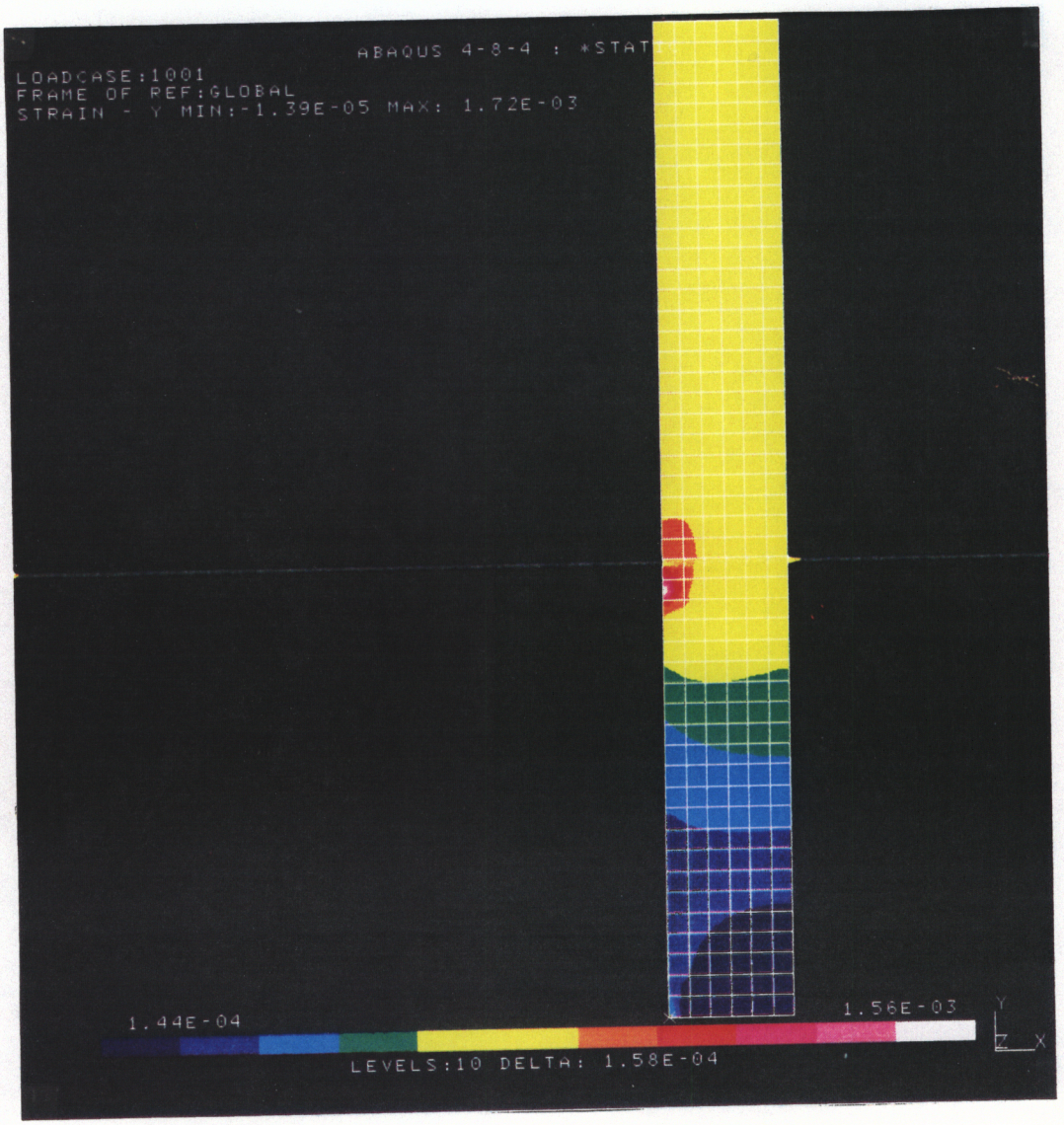

Figure 3-2 Strain Contour with Tension Load of 20 kips

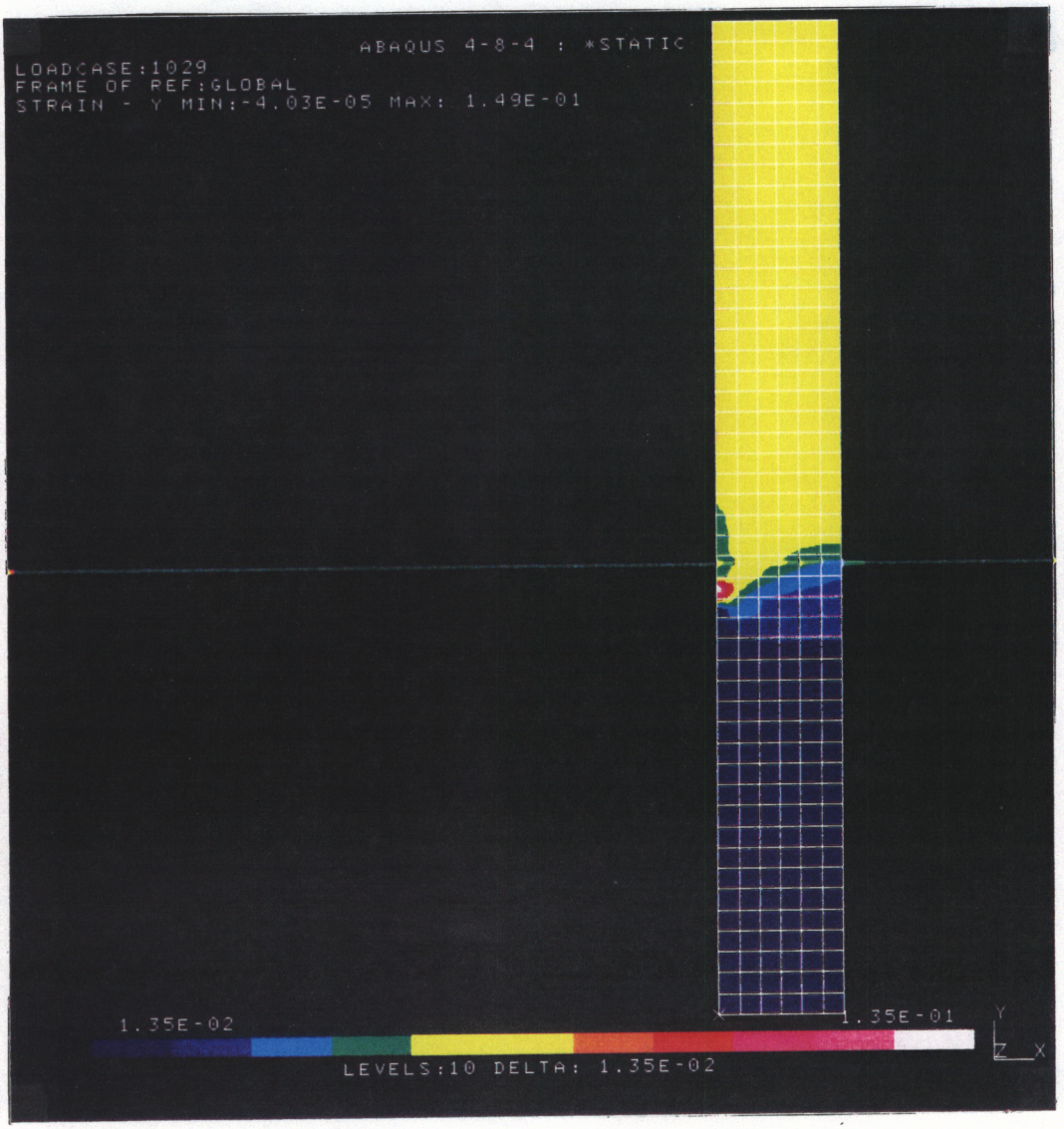

Figure 3-3 Strain Contour with Tension Load of 54.7 kips

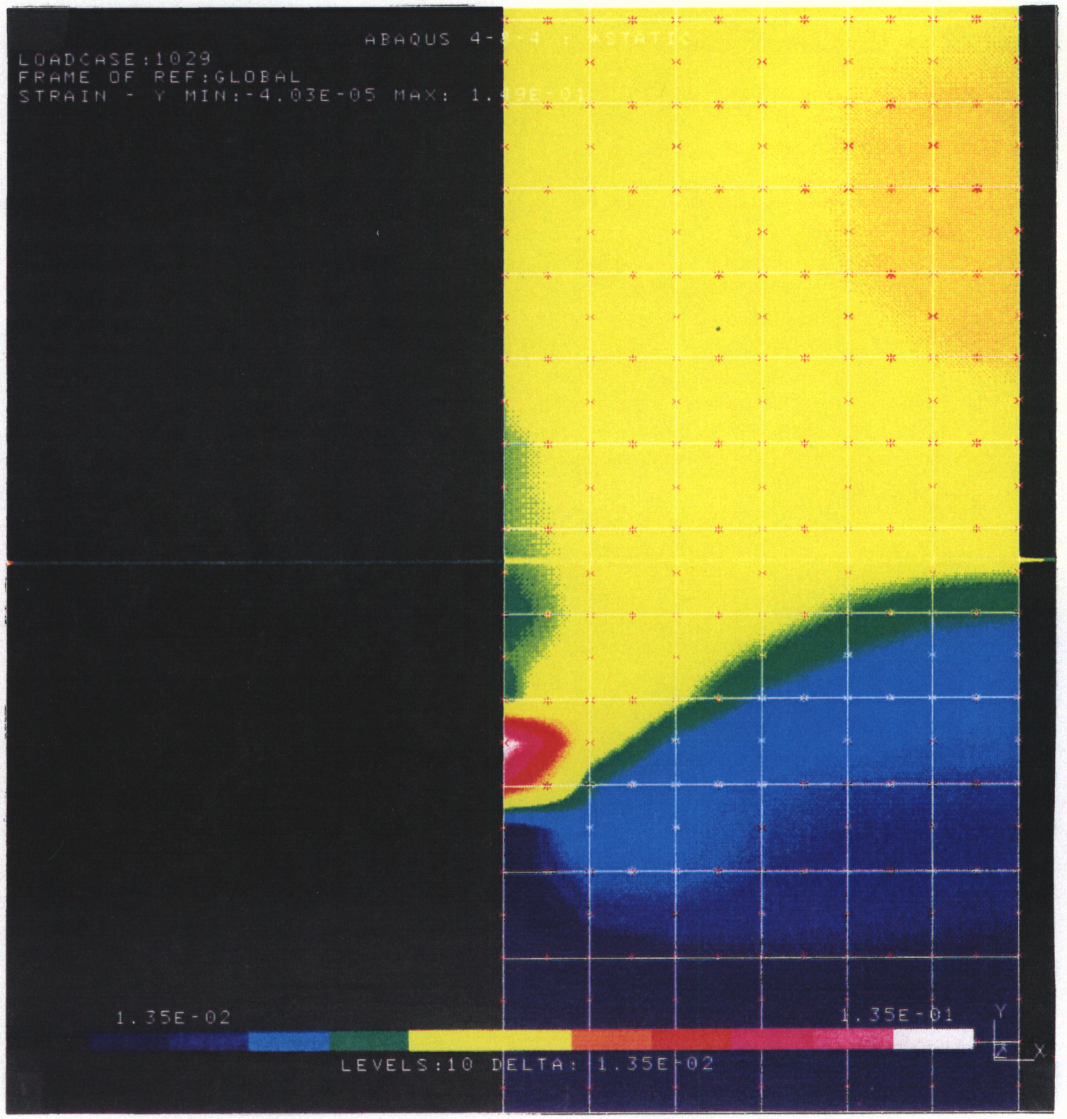

Figure 3-4 Local Enlargement of Critical Section

for the Strain Contour in Figure 3-3

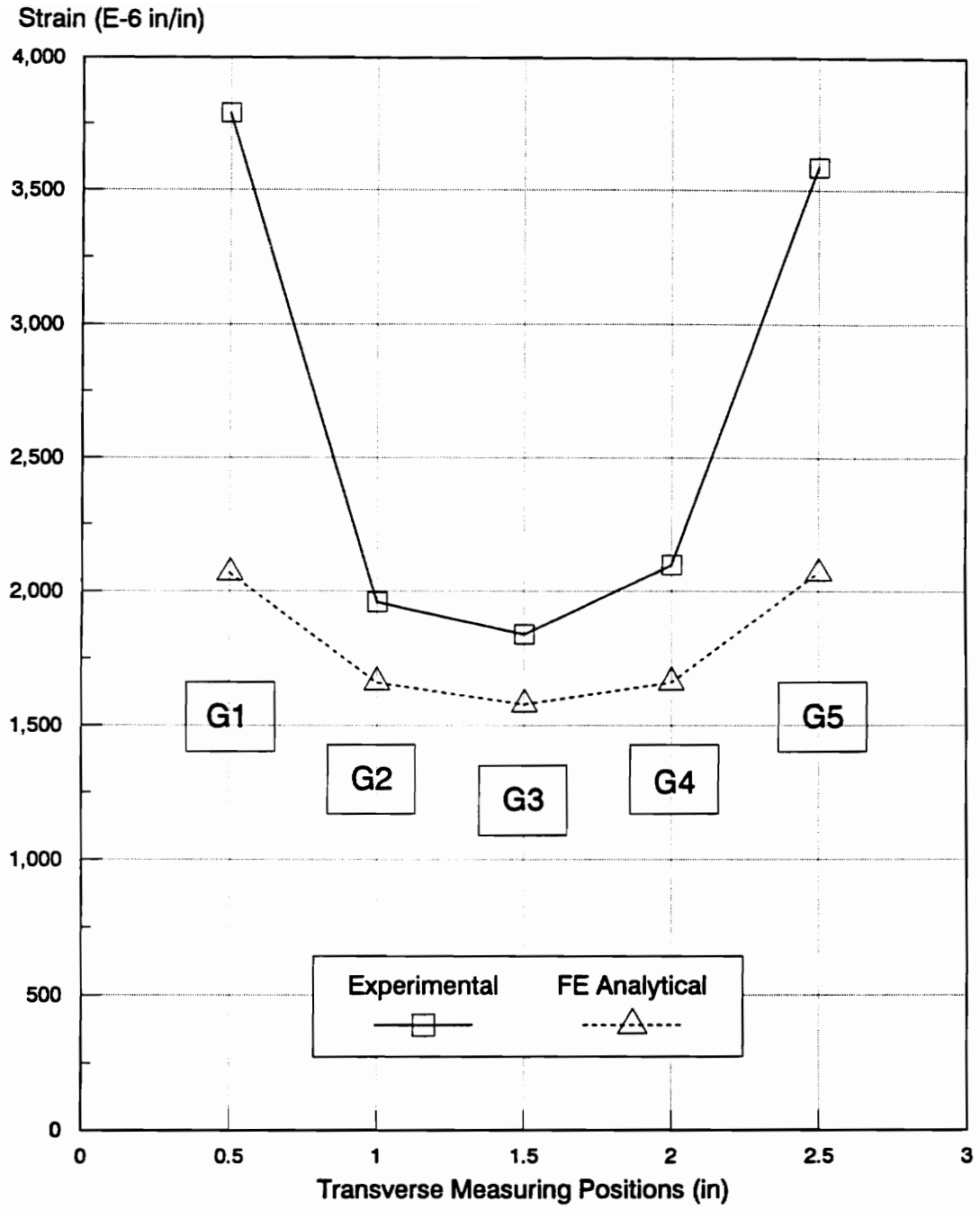

Figure 3-5 Strain Comparison: Experimental vs. Analytical, Load = 45 kips

2. With a load of 52.5 kips applied to the experimental specimen, the strain concentrates on the G5 side of the plate. And when the load increases to 55 kips, the strain further concentrates on the G5 side, but the strain value for G4 becomes abnormally low. This overwhelming concentration of strain at G5 indicates that a failure (in the form of a crack) has already begun, originating at the critical section on the G5 side. The possible explanations for the strain concentration include:
   a. A nonsymmetric applied tension load, which in this case has more load applied to the G5 side. This may be caused by a slip of the test machine's grasp of the gusset plate.
   b. A sudden fracture failure at the critical section in the vicinity of G5. This may be due to a small flaw or a notch made during end-welding.
   c. Unbalanced welding strength of the two sides of the plate.
3. In the analytical model the distribution of the tension load and the geometry are symmetric, therefore, the strain distribution is symmetric as well.
4. The analytical strain values are slightly smaller than their corresponding experimental values when the load cases are below 50 kips.
5. In the Fig. 3-6, the analytical strain diagrams of the three load stages (53.6, 54, 54.6, and 54.7 kips) are compared with the strain diagram for the experimental ultimate load (55 kips). According to Table 3-1, the largest analytical load is 54.7 kips. Since the failure of the plate specimen is caused by the extreme strain concentration at the critical section near gage G5, thus, when the analytical strain value, under the largest load conditions, reaches the largest experimental value, the failure of the plate is pointed out. Accordingly, the analytical ultimate load is therefore the largest load, 54.7 kips.

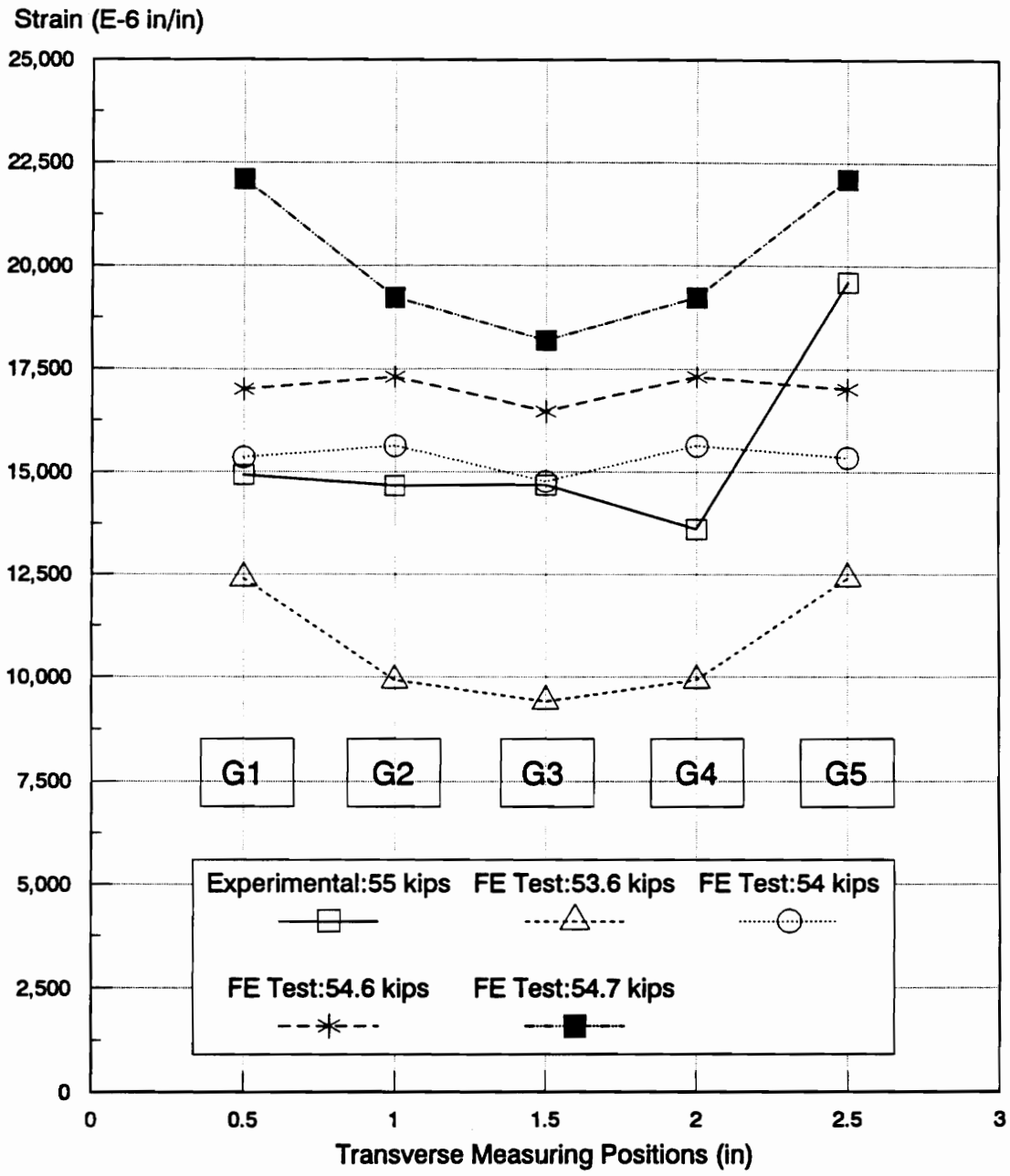

Figure 3-6 Strain Comparison: Experimental Data and Various Analytical Data Sets

Chapter 4 Analysis of Eccentric Loads

4.1 General

In Chapter 3, an unusually large experimental strain value was observed. Potential sources of this phenomenon are nonsymmetric applied tension load or unbalanced welding strength (see section 3.3). Eccentric load effects are the focus of this chapter. Three types of load eccentricity are investigated in this analysis. They are listed as follows :

1. ECC1, Eccentricity = 0.25 in.
2. ECC2, Eccentricity = 0.50 in.
3. ECC3, Eccentricity = 0.75 in.

A full FE mesh (half of the test plate) is built for this investigation because of the lack of symmetry. This mesh has 21 spring groups on each side simulating the welds. While the lower portion of the plate model remains square refined, as in Chapter 3, the

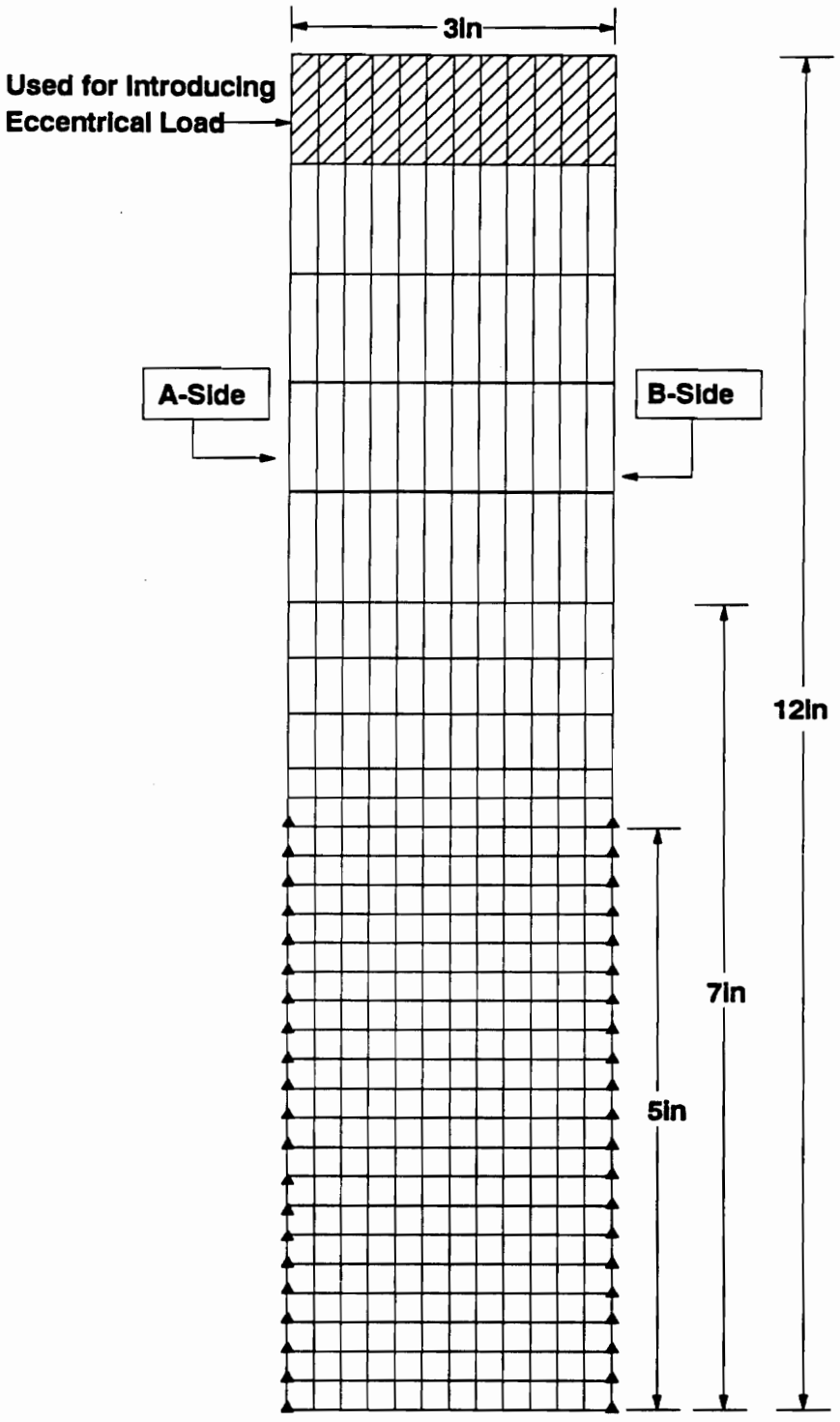

Figure 4-1 The FE Mesh for Eccentric Load Study

upper portion of the plate model is less refined because no critical condition is expected to occur in this area. The illustration of this mesh is shown in Fig. 4-1.

4.2 Arrangement of the Eccentric Loads

Originally, the tension load is defined by uniformly distributed point forces. However, since the real condition of the eccentric load is complex and unknown, the following assumptions are made:

1. The eccentricity is caused by an off center load or by unbalanced welding. The eccentric resultant load is moved a certain distance toward the A side (see Fig. 4-1).
2. This load is uniformly distributed over a small portion of the plate, and the resultant load vector is located just at end of the eccentric load area (see Fig. 4-2). The distribution is represented by a shaded area instead of points.
3. This extra load is proportionally relative (i.e., differing by a constant c) to the point loads assumed in the initial model.
4. The transverse neutral-line remains straight and normal to the Y axis until the plate fails.

Based on the above assumptions, the load propotional relations are calculated as follows:

Eccentricity = 0.25 in. Illustration is given in Fig. 4-2.

F_{y1} = original point force at each node of side;

F_{y2} = extra force applied at each side element;

F_{Y1} = total original point forces;

F_{Y2} = total extra force;

F_{Total} = resultant load;

$F_{Total} = F_{Y1} + F_{Y2} = 5F_{y1} + 48F_{y2}$;

$F_{Total}\,(1.5 + 0.25) = F_{Y2}\,(2.375) + F_{Y1}\,(1.5)$;

$(5F_{y2} + 48F_{y1})\,(1.75) = 5F_{y2}\,(2.375) + 48F_{y1}\,(1.5)$;

$8.75F_{y2} + 84F_{y1} = 11.875F_{y2} + 72F_{y1}$;

$12F_{y1} = 3.125F_{y2}$;

$\boldsymbol{3.84F_{y1} = F_{y2}}$.

The values for the 0.5 inch and 0.75 inch eccentricity are found in a similar way. The results are

Eccentricity = 0.5 in.

$\boldsymbol{12F_{y1} = F_{y2}}$.

Eccentricity = 0.75 in.

$\boldsymbol{32F_{y1} = F_{y2}}$.

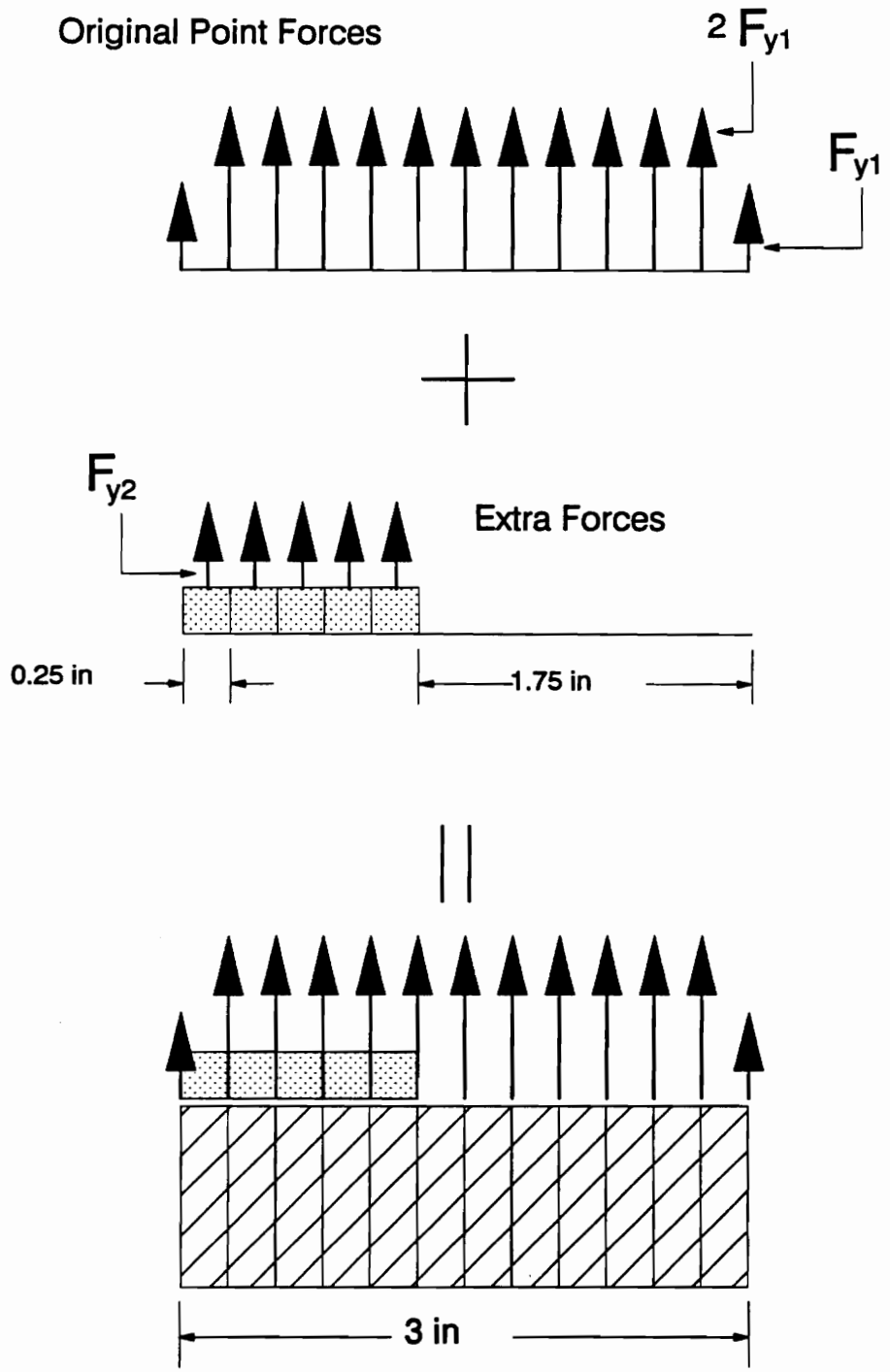

Figure 4-2 Generation of Eccentric Load with Eccentricity = 0.25

4.3 Results

Three cases of eccentricity, ECC1, ECC2 and ECC3, were evaluated to survey the effect of an eccentric load. The FE calculations of all the three cases end because of the input limitation (see section 2.3). As a result, the last load values found are recognized as the ultimate loads, which are 55 kips for ECC1, ECC2, and ECC3. Based on this analytical data, load vs. displacement diagrams for ECC1, ECC2, and ECC3 are produced and compared with the experimental data (see Fig. 4-3). They indicate very small load differences among these eccentric cases and general model. This figure also shows the ultimate load values of experimental test and the other FE models are quite similar while the difference of displacement between the experimental test and FE models is large.

To investigate how much the eccentricity influences the strain distribution inside the plate, strain comparison figures focusing on the positions G1 to G8 are shown in Figs. 4-4 and 4-5, with the load value fixed at 52 kips. These two figures also include the strain data from the general model (denoted by eccentricity = 0 inch) and the experimental test. From the figures, ECC1 model (its eccentricity = 0.25 inch) appears the closest in its characteristics to the experimental values. The ECC3 model appears to have unusually low strain values, which implies that the load transmission is strongly limited by the large eccentricity and the special boundary condition (recall the assumption of transverse neutral line in section 4.2).

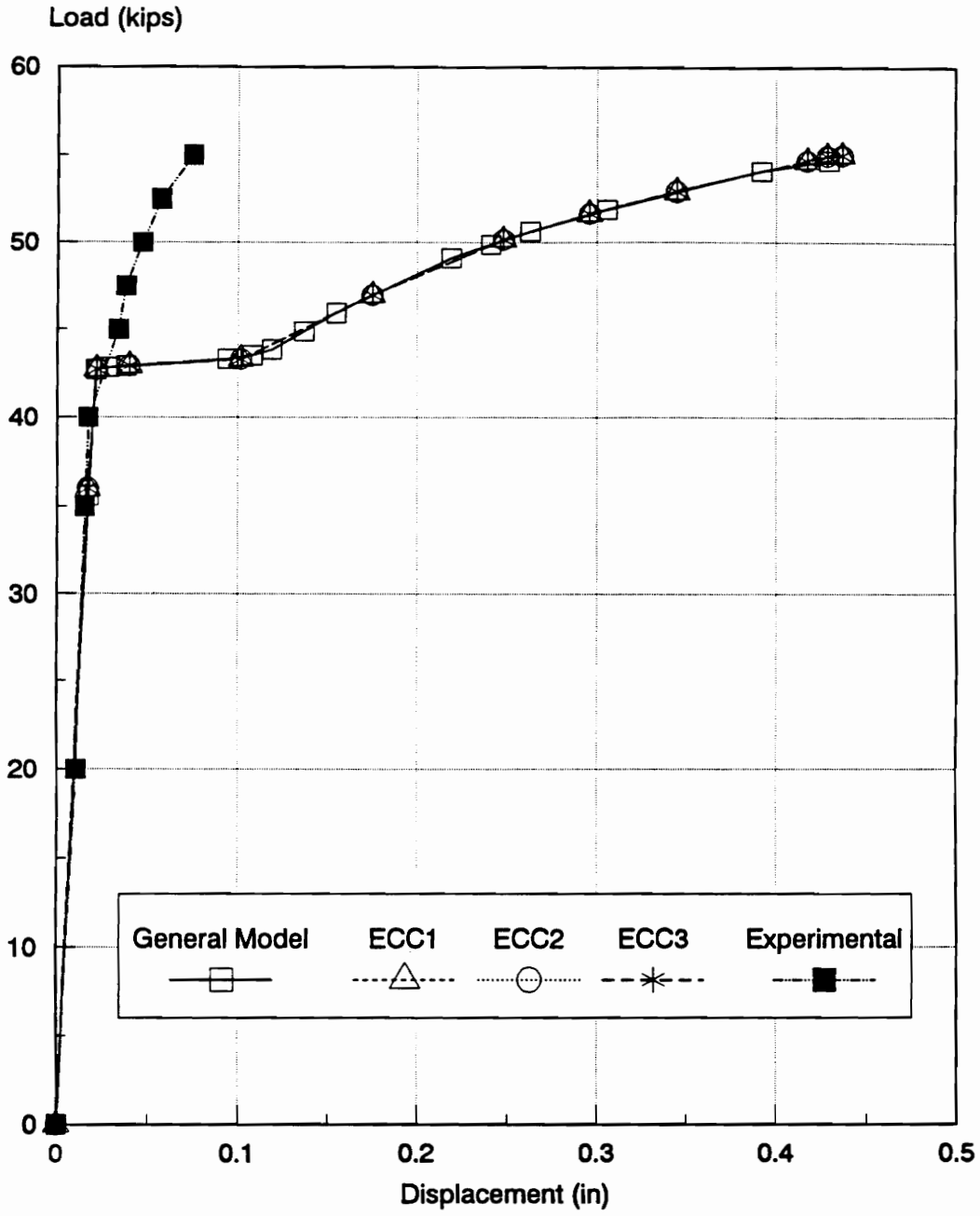

Figure 4-3 Load-Displacement Diagrams of Various Eccentric Model, General Model and Experimental Test

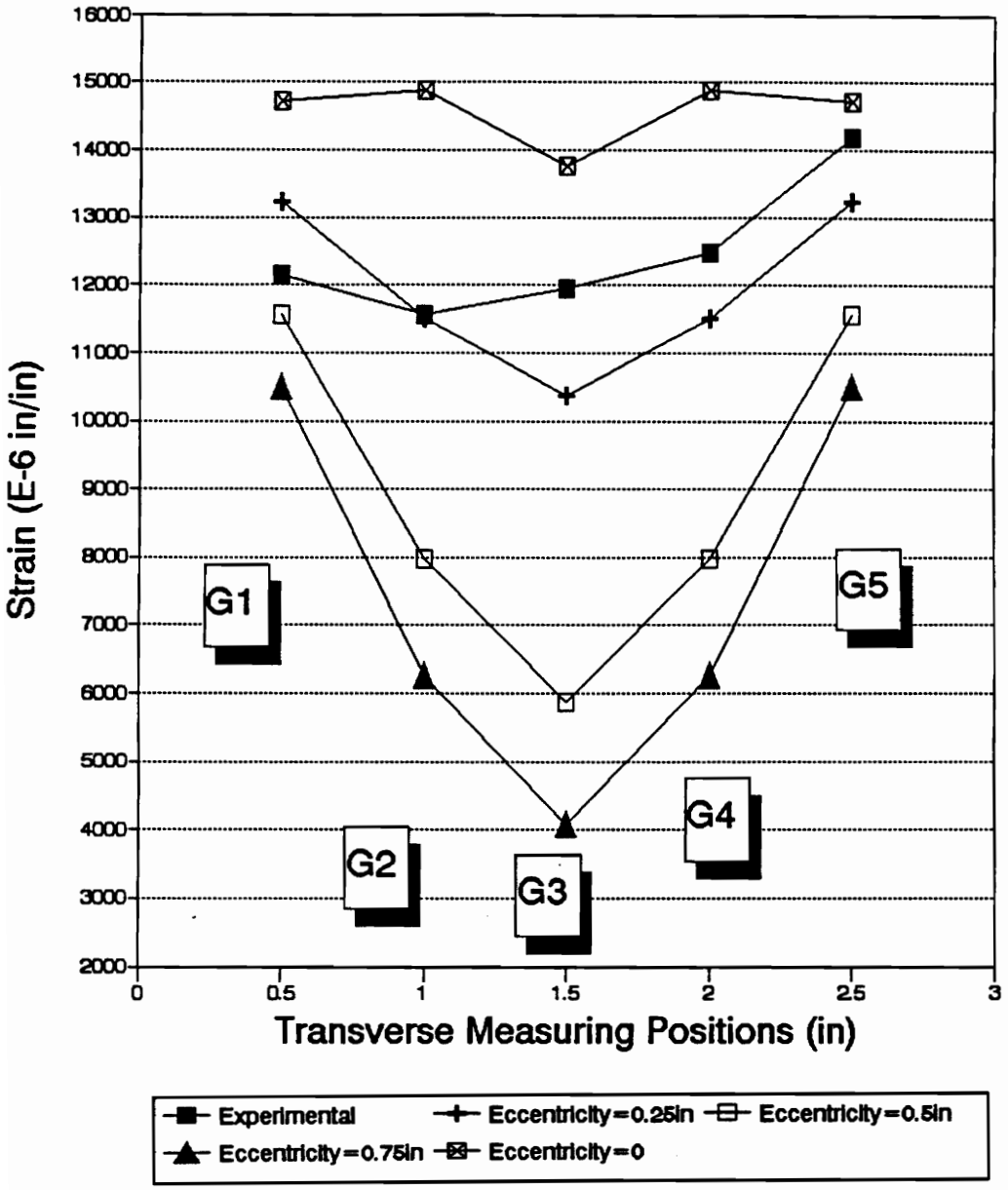

Figure 4-4 Strain Comparison for Transverse Positions:

Experimental vs. Analytical, Load = 52.5 kips

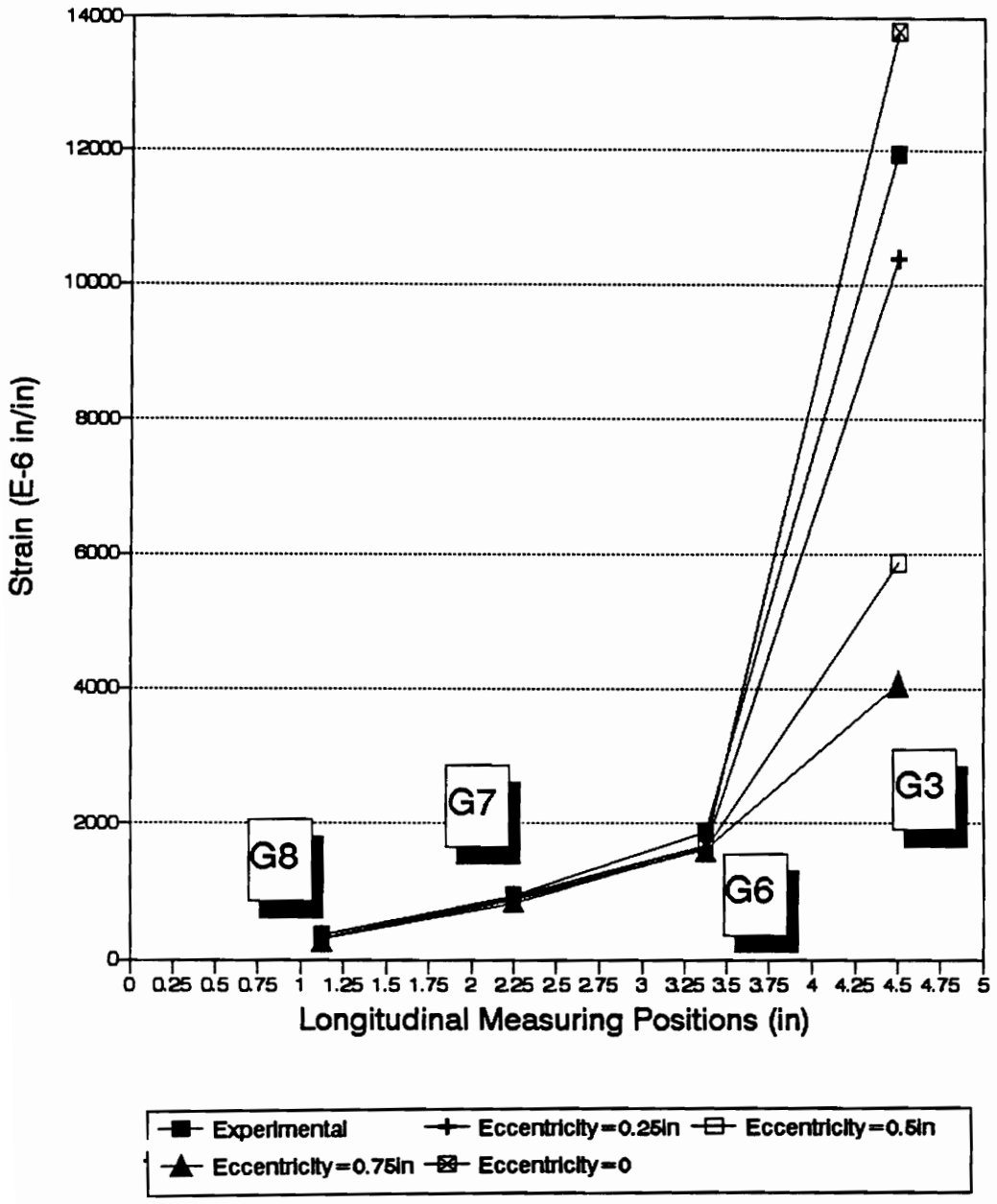

Figure 4-5 Strain Comparison for Longitudinal Positions:

Experimental vs. Analytical, Load = 52.5 kips

Two strain contours are given in Figs 4-6 and 4-7 to show the eccentric effect on the whole plate. Figure 4-6 is related to the strain contour of ECC2 with its ultimate load. In this figure, eccentric effect is not obvious. Most of the strain is distributed symmetrically. Figure 4-7 is related to the strain contour of ECC3 with its ultimate load. In this figure, strains concentrate in three areas, the two critical sections and the upper brown section. The maximum tension strain value is found at the critical section (0.125 inch out from the end spring) on the B-side. This phenomenon shows that the upper part of the B-side needs to be elongated to offset the loss of deformation caused by the rotation referred to in the former paragraph. This elongation results in the tension strain concentrated at the critical section of B-side .

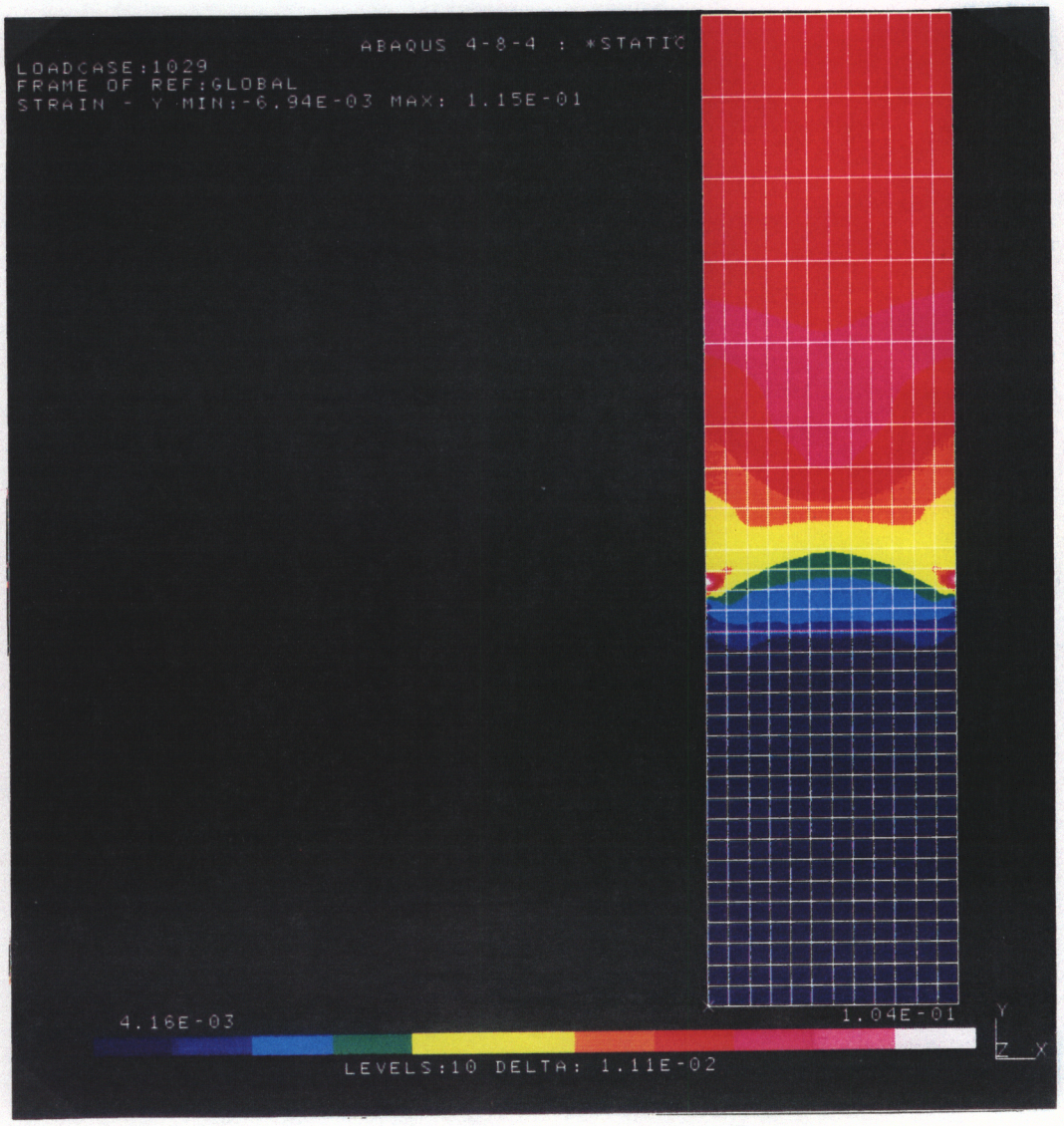

Figure 4-6 Strain Contour of ECC2 Under Its Ultimate Load

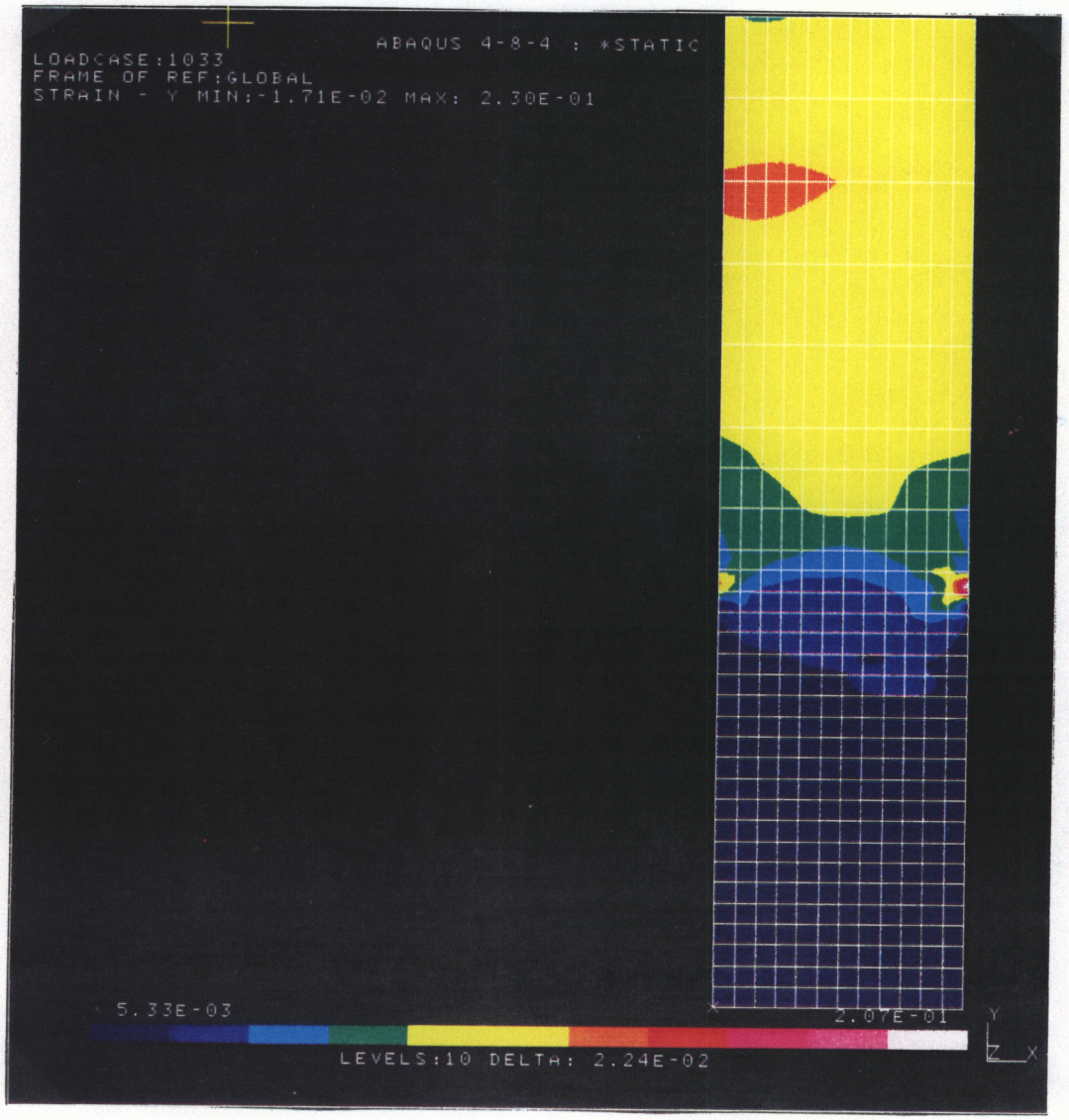

Figure 4-7 Strain Contour of ECC3 Under Its Ultimate Load

Chapter 5 Analysis of Notched Plate

5.1 General

An imperfection, or notch, caused by starting or stopping of the welding process may cause a decrease of the tension strength of the plate members. In this chapter, two different sizes of notches are considered. Two notched-plate FE meshes are developed. Nonlinear analyses are conducted on these meshes.

5.2 Notch Description

Notches are assumed to be triangular and located on the critical section. The first notch, Notch1 model, is 1/8 inch wide at the bottom, and 1/16 inch deep, as shown in Fig. 5-1. The second notch, Notch2, is the same width at the bottom, but 1/8 inch deep, as

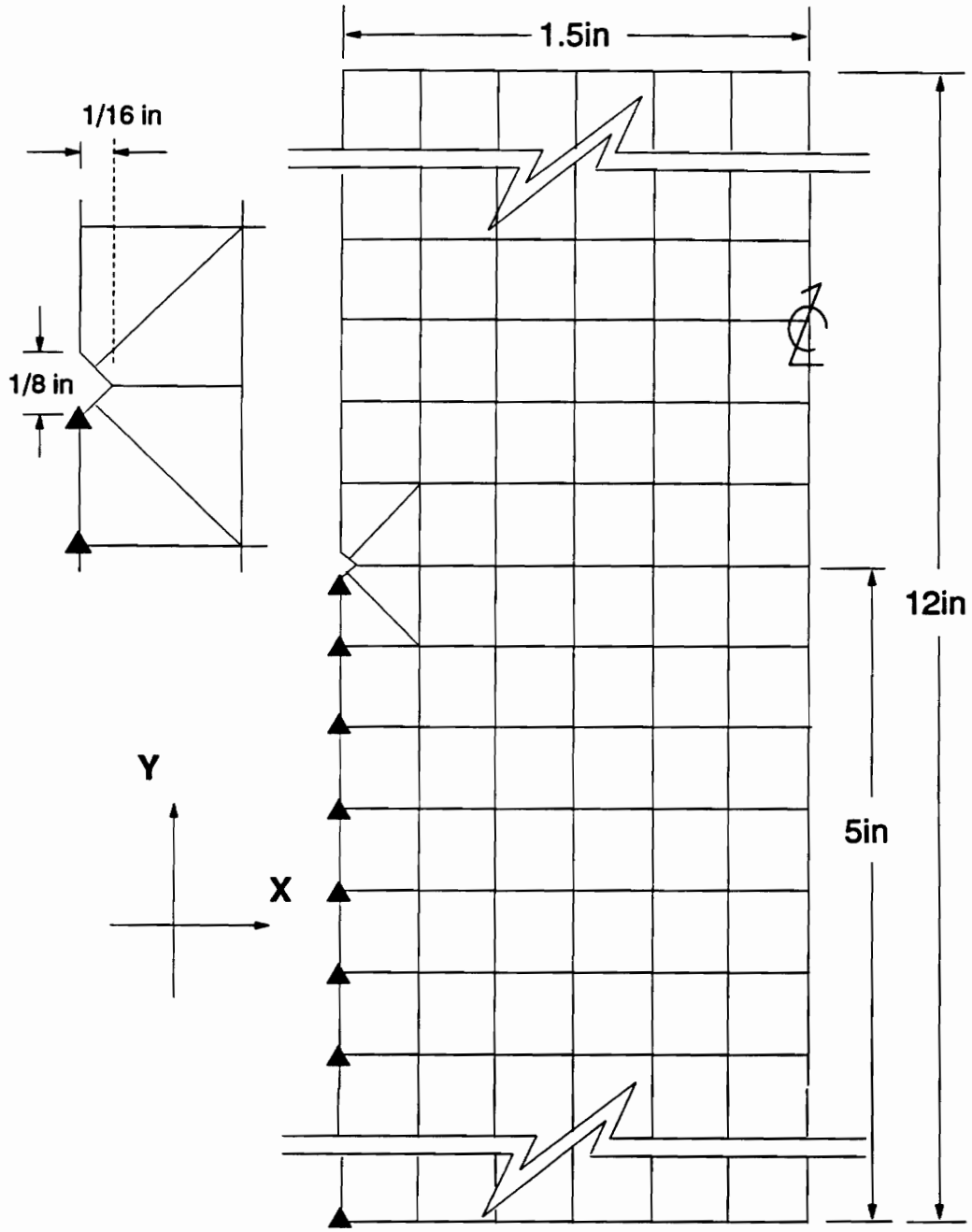

Figure 5-1 Illustration of Critical Section of Notch1

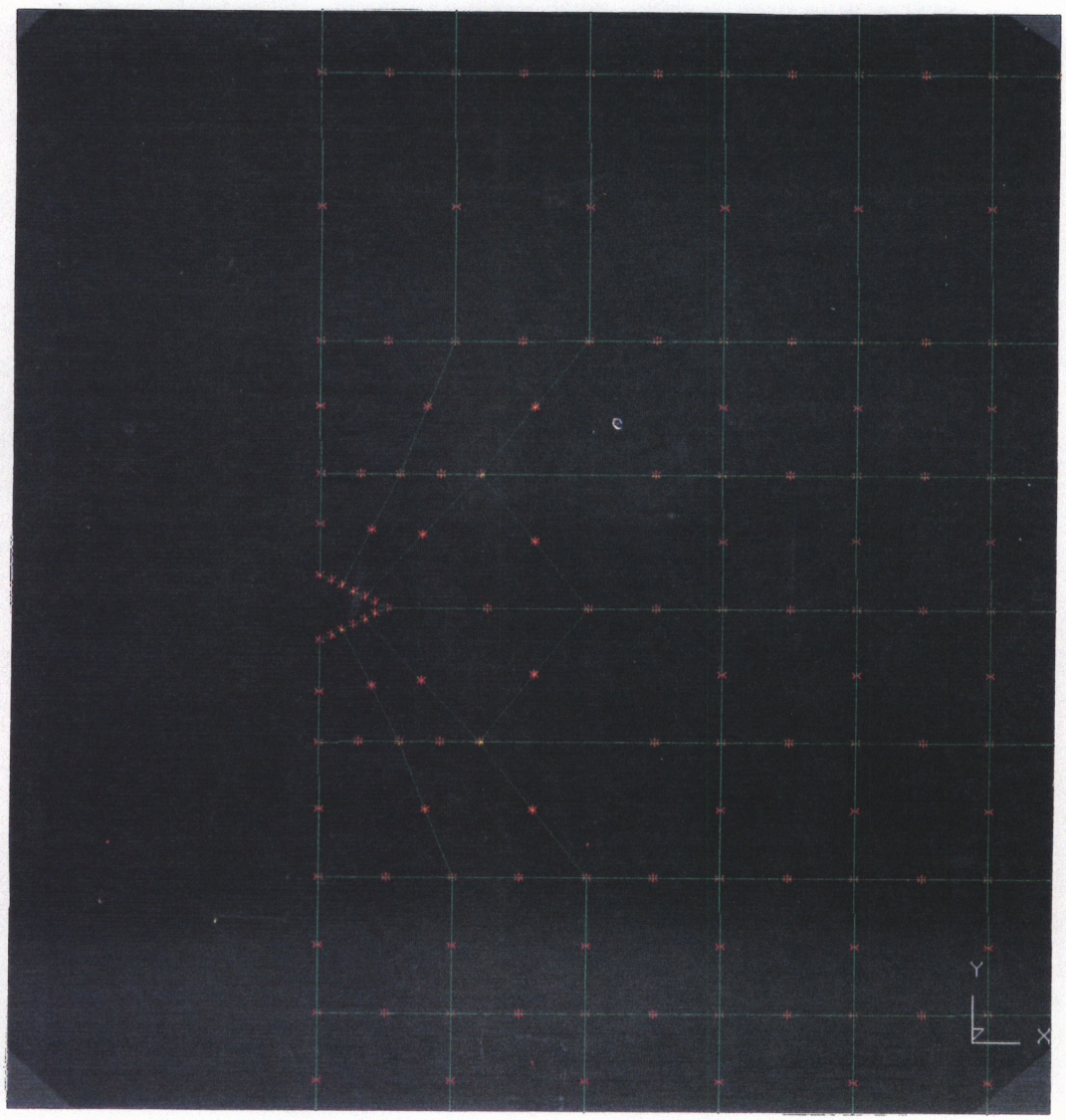

Figure 5-2 Illustration of Critical Section of Notch2

shown in Fig. 5-2. The position of the end welds, represented by the last spring group, moves downward 1/16 inch due to the presence of the notch.

5.3 Notched-Plate FE Mesh

For the 1/16 inch deep notch, four special CPS8 elements are arranged to surround the notch. All other elements are the same as the corresponding ones in the general model. In the four special CPS8 elements, every interior angle is carefully arranged not to be less than 45 degrees or greater than 135 degrees, so the isoparametric problems can be avoided.

For the 1/8 inch deep notch, a total number 14 elements are arranged for the same purpose. The meshes of these two notch models are examined by IDEAS to make sure no geometry problems may be occured.

5.4 Results

A load vs. displacement diagram of both notch models is shown in Fig. 5-3. The ultimate loads of the Notch1 and Notch2 models are 42.336 kips, and 43.392 kips, respectively. The Notch2 model is more flexible than the Notch1 model.

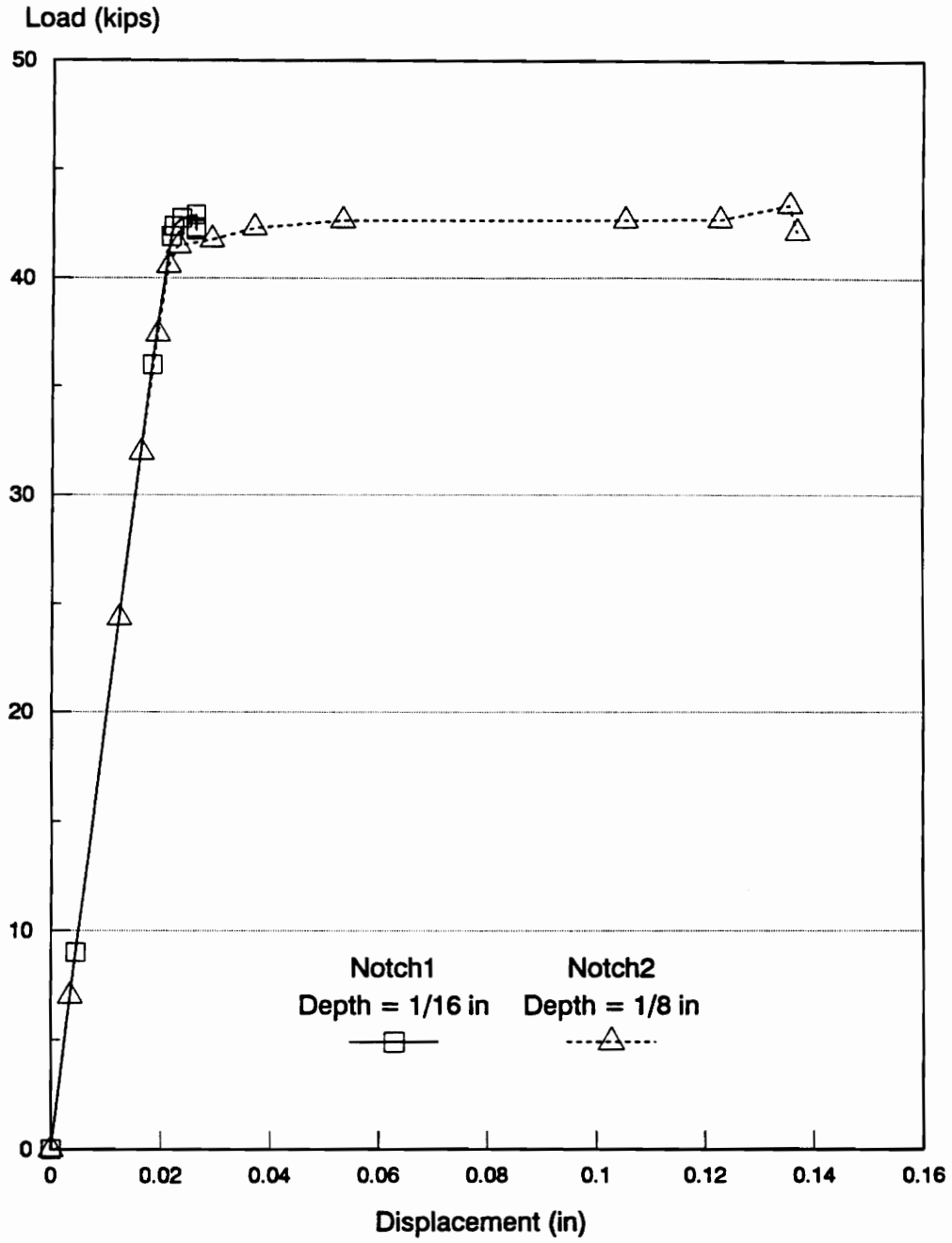

Figure 5-3 Load-Displacement for Notch Models

Two points may be obtained from observing these two models:

1. The tension strength of the plate may be dramatically decreased by notches when compared with the general model, whose ultimate load is 54.7 kips.
2. The depth of the notches, based on the limited variation studied, does not influence the plate strength much, but it does influence the flexibility of the plate.

Chapter 6 Determination of Shear Lag Coefficient

6.1 Arrangement of Case Study

In Chapter 2, a general plane FE model, is produced and shown to be reliable by a convergence examination. In Chapter 3, it is found that this general FE plate model may provide strain and load values which are close to experimental findings. Accordingly, the case studies of the shear lag coefficient are conducted by changing the welding length of this general FE plate model. Eccentric conditions and notch conditions are not included in this case study.

The calculation of the shear lag coefficient in LRFD Specification is given by:

(a) when $l > 2w$ $U = 1\ 00$;

(b) when $2w > l > 1.5w$ $U = 0.87$;

(c) when $1.5w > l > w$ $U = 0.75$.

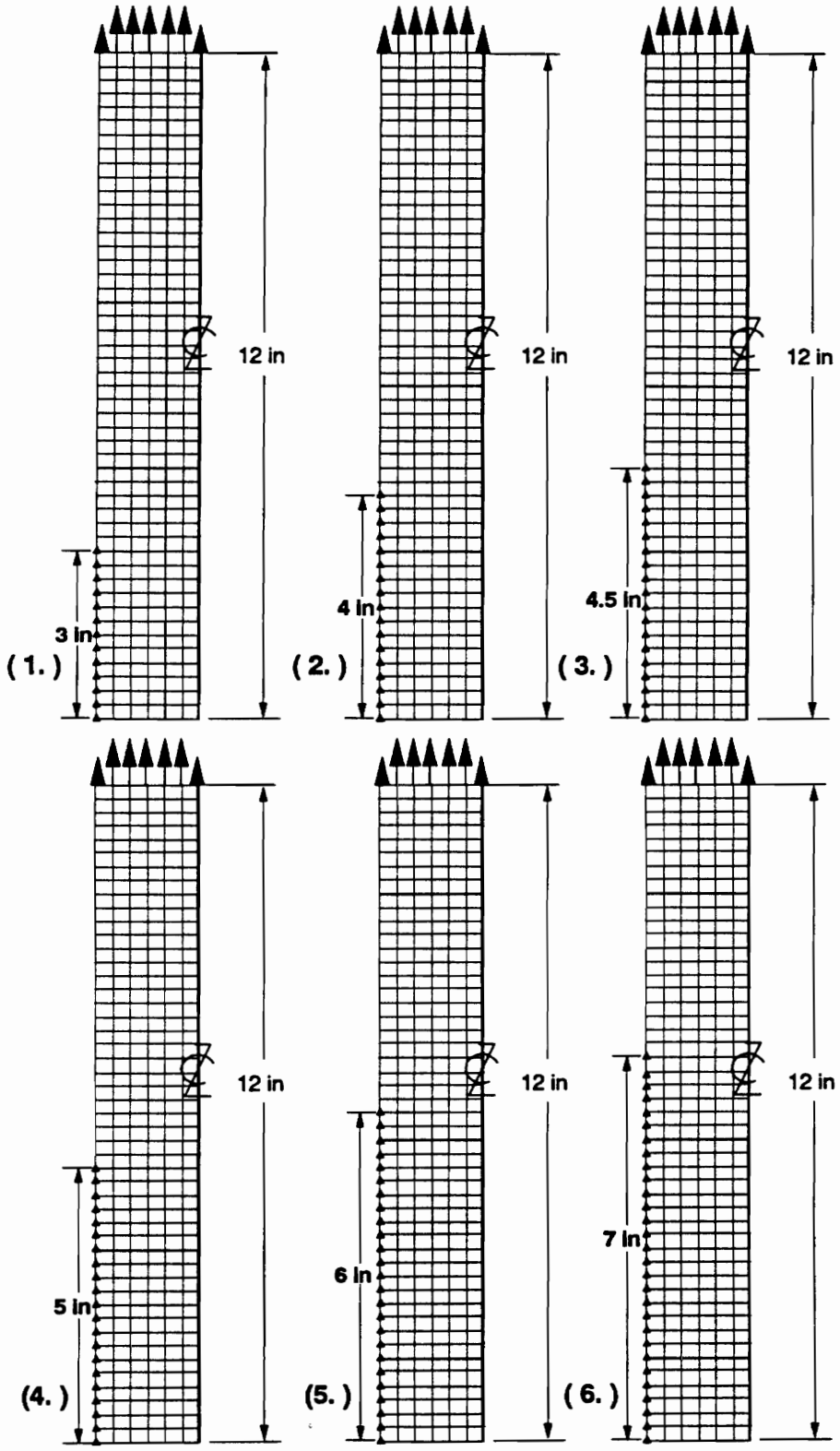

Figure 6-1 Illustration of FE Models Used in Investigation

Based on the above partitions, three investigation groups are designed. Each one includes two FE models; their corresponding illustrations are given in Fig 6-1. Every model is 1/4 part of the plate. The three investigation groups are as follows:

1. Case1, $1.5w > l \geq w$. The weld lengths are assigned to be 3 inches (1.) and 4 inches (2.), respectively.
2. Case2, $2w > l \geq 1.5w$. The weld lengths are assigned to be 4.5 inches (3.) and 5 inches (4.).
3. Case3, $l \geq 2w$. The weld lengths are assigned to be 6 inches (5.) and 7 inches (6.).

6.2 Results

Load and displacement data are acquired from the ABAQUS mainout files and shown in Fig. 6-2. This figure indicates that: (1) the models with the longer weld lengths have slightly greater strength than the ones with the smaller weld lengths. The load values are also given in Table 6-1; and (2) the models maintain similar ductility regardless of the length of the welds.

Table 6-1 Case Study: Ultimate Load of Every Case

Investigation Group	Case 1		Case 2		Case 3	
Model Number	(1)	(2)	(3)	(4)	(5)	(6)
Weld Length (in)	3	4	4.5	5	6	7
Ultimate Load	52.7	54.1	54.7	54.7	54.8	54.9

The recording for each model stops immediately after the maximum load is found. Every analysis run ends because the limitation of PTOL (see section 2.3).

6.3 Comparison of Shear Lag Coefficients

Recalling the LRFD code, the shear lag coefficient, U, of the member depends on its width w and its welding length l; this definition is given by the following relationship:

$$A_e = UA_g,$$

where A_e = effective cross-sectional area;

A_g = gross cross-sectional area;

and $U = 1.0$ when $l > 2w$;

$U = 0.87$ when $2w > l > 1.5w$.

$U = 0.75$ when $1.5w > l > w$.

In this study, the dimensions of the plate specimen satisfy the second condition; thus the code-regulated coefficient, U_{code}, is 0.87.

The experimental ultimate tension stress, σ_u, calculated from the coupon test data, is 76.6 ksi. Therefore, the calculated ultimate tension load is calculated as follows:

$$F_u = \sigma_u \times A = (76.7) \times (3 \times 0.259) = 59.6 \quad \text{kips.}$$

The experimental ultimate load, $F_{u\text{-}exp}$, was 55 kips (given in Appendix A). Therefore, the experimental shear lag coefficient is determined as follows:

$$U_{\text{experimental}} = \frac{F_{u-exp}}{F_u} = \frac{55}{59.6} = 0.92$$

The analytical shear lag coefficient for the weld length of 5 inches is calculated as follows:

$$U_{\text{analytical}} = \frac{F_{u-analytical}}{F_u} = \frac{54.7}{59.6} = 0.92$$

Similar calculations produce shear lag coefficients for the other weld lengths, see Table 6-2.

Table 6-2 Shear Lag Coefficient Derived for Each Case

Investigation Group	Case 1		Case 2		Case 3	
Model Number	(1)	(2)	(3)	(4)	(5)	(6)
Ultimate Load	52.7	54.1	54.7	54.7	54.8	54.9
Shear Lag Coefficient ($U_{analytical}$)	0.88	0.91	0.92	0.92	0.92	0.92

Comparing the outcome of the above calculations, the code, experimental, and analytical coefficients are related in the following way:

(A) With the weld length of 5 inches:

$$U_{\text{experimental}} (= 0.92) = U_{\text{analytical}} (= 0.92) > U_{\text{code}} (= 0.87).$$

(B) When $l > 2w$;

$U_{code} = 1.0$, $U_{analytical} = 0.92$;

$U_{code} > U_{analytical}$.

(C) When $2w > l > 1.5w$;

$U_{code} = 0.87$, $U_{analytical} = 0.92$;

$U_{code} < U_{analytical}$.

(D) When $1.5w > l > w$;

$U_{code} = 0.75$, $U_{analytical} = 0.88 \sim 0.92$;

$U_{code} < U_{analytical}$.

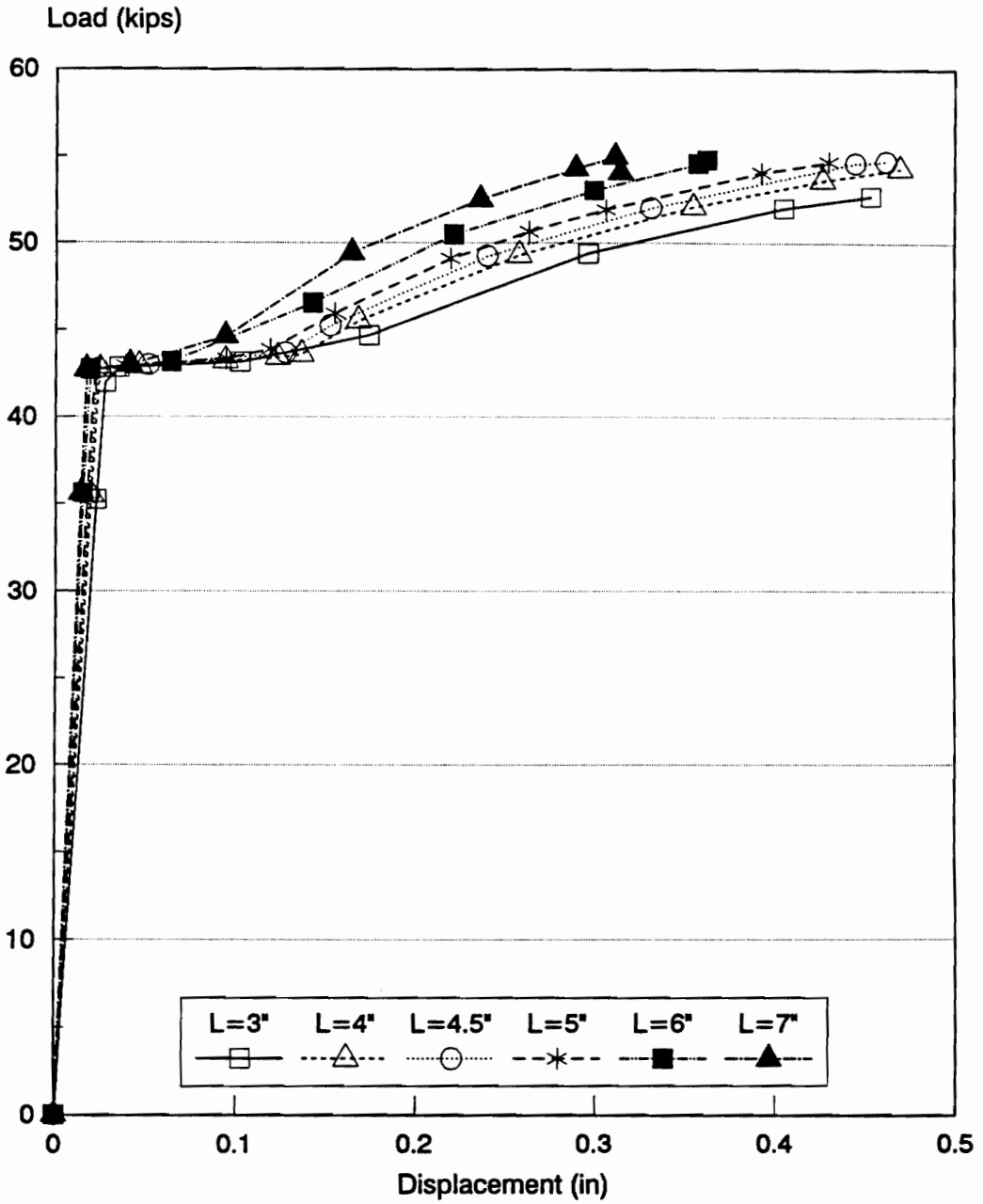

Figure 6-2 Load-Displacement for FE Models of Different Weld Lengths

Chapter 7 Conclusions and Recommendations

7.1 Conclusions

Based on the analytical investigations conducted, the following conclusions are drawn:

1. Due to shear lag problems, the analytical ultimate tension strength of the plate member under general circumstances (that is, when no eccentricity or notches exist) is quite close to the experimental strength, but more conservative.

2. Eccentric load conditions may cause rotated deformations whose magnitudes depend on the amount of eccentricity.

3. Due to the combined effect of eccentricity and the special limitation requiring that the transverse neutral line remain horizontal, the critical spot of the maximum strain concentration is found at the weld side farthest from the resultant eccentric load.

4. Very small notches caused by the welding may dramatically decrease the tension strength of plate members. The depth of a notch seems to be more important for the ductility rather than for the strength.

5. For plates connected by only longitudinal welds, connection length is shown to have very little influence on the shear lag coefficient. The analytical shear lag coefficients change from 0.88 to 0.92, when the lengths of welds change from 3 inches to 7 inches and the widths of the plates remain at 3 inches. This implies that an upper limit on the shear lag coefficient of 1.0 is not appropriate. Regardless of the length of the weld, a stress concentration will always exist thereby reducing the effectiveness of the tension member.

7.2 Recommendations

1. An upper limit on the shear lag coefficients of 0.9 is recommended for design.

2. A three-dimensional FE model should be built for investigating the effects due to the changing of the plate's thickness.

3. Differences exist between the displacement values of the experimental test and the FE approach under ultimate load conditions. Further investigations are necessary to find the reasons for these differences.

4. The stiffness of the welds needs to be investigated experimentally, so as to allow for more accurate FE approaches in future analyses.

BIBLIOGRAPHY

ABAQUS, General-Purpose Finite Element System, Hibbit, Karlsson and Sorensen, Inc., 100 Medway Street, Providence, RI 02906, U.S.A.

Bathe, K. J. (1982), *Finite Element Procedures in Engineering Analysis*, Prentice-Hall, Englewood Cliffs, NJ.

Beaulieu, D. and Picard, A. (1988). *Finite element modeling of connections*, Connections in Steel Structures: Behavior, Strength, and Design, R. Bjorhovde et. al., eds., Elsevier Applied Science Pub., New York, NY.

Butler, L. J. and Kulak, G. L. (1971). *Strength of fillet welds as a function of direction of load*, Welding Journal, 50(5), 231s-234s.

Cook, R. D., Malkus, D. S., and Plesha, M. E. (1989). *Concepts and Applications of Finite Element Analysis*, 3rd edition, John Wiley and Sons.

Crisfield, M. A. (1986). *Finite Elements and Solution Procedures for Structural Analysis*, Vol 1: Linear Analysis, Pineridge Press Limited, Swansea, U.K.

Engineering for steel constructions: a source book on connections, (1984). American Institute of Steel Construction, Inc. (AISC), Chicago, IL.

I-DEAS, Engineering Analysis, Model Solution, and Optimization, Macneal-Schwendler, Structural Dynamics Research Corporation, 2000 Eastman Drive, Milford, Ohio, U.S.A.

I-DEAS, Engineering Analysis, Tdas. Test Data Analysis, Macneal-Schwendler, Structural Dynamics Research Corporation, 2000 Eastman Drive, Milford, Ohio, U.S.A.

Gonzalez, L. and Easterling, W. S. (1989). *Investigation of The Shear Lag Coefficient for Welded Tension Members*, Virginia Polytechnic Institute and State University, December 1889.

Load and resistance factor design specification for structural steel buildings, (1986), American Institute of Steel Construction, Inc. (AISC), Chicago, IL.

Pisarski, H.G. (1985). *Philosophy of Welded Wide Plate Testing for Brittle Fracture Assessment:*, Fracture Mechanics of Welds, Blauel, J. G. and Schwalbe, K. H., Mechanical Engineering Pub., London, U.K., 191-208.

Richard, R. M., Rabern, D. A., Hormby, D. E., and Williams ( ), G. C. Analytical Models for Steel Connections, Behavior of Metal Structures, Hall, W. J. and Gaus, M. P., ASCE, New York, N.Y., 128-154.

Robino, C. V., Dias R. J., Varughese R., and Pense (1987), A. W. *The Fracture Behavior of A588 Grade A and A572 Grade 50 Weldments*, Lehigh University, Bethlehem. Welding Research Council Bulletin n330, Jan 1988, 1-10.

APPENDIX A

Experimental Data (Gonzalez and Easterling 1989)

Table A-1

Experimental Strain Data for Plate Specimen P-L2-2; Strain Unit = E-6 in/in; Load Unit = kips.									
Load	Gage 1	Gage 2	Gage 3	Gage 4	Gage 5	Gage 6	Gage 7	Gage 8	Displacement
0	0	0	0	0	0	0	0	0	0
10	485	370	351	362	431	289	181	73	0.0075
20	1,091	760	703	721	857	560	340	141	0.0105
30	1,905	1,191	1,068	1,099	1,351	872	520	215	0.014
35	2,455	1,483	1,263	1,299	1,674	1,059	620	254	0.0155
37.5	2,821	1,671	1,396	1,420	1,886	1,169	671	273	0.0165
40	2,887	1,721	1,458	1,503	2,069	1,156	642	253	0.0175
42.5	2,976	1,832	1,634	1,819	2,623	1,285	696	276	0.0285
45	3,789	1,960	1,840	2,097	3,588	1,379	723	274	0.034
47.5	4,392	2,119	2,007	2,319	4,549	1,500	783	296	0.038
50	7,690	4,430	3,943	4,547	8,597	1,690	856	319	0.047
52.5	12,147	11,580	11,944	12,490	14,198	1,876	926	343	0.0575
55	14,930	14,673	14,688	13,604	19,611	2,058	1,006	377	0.075

(Gonzalez, p.146)

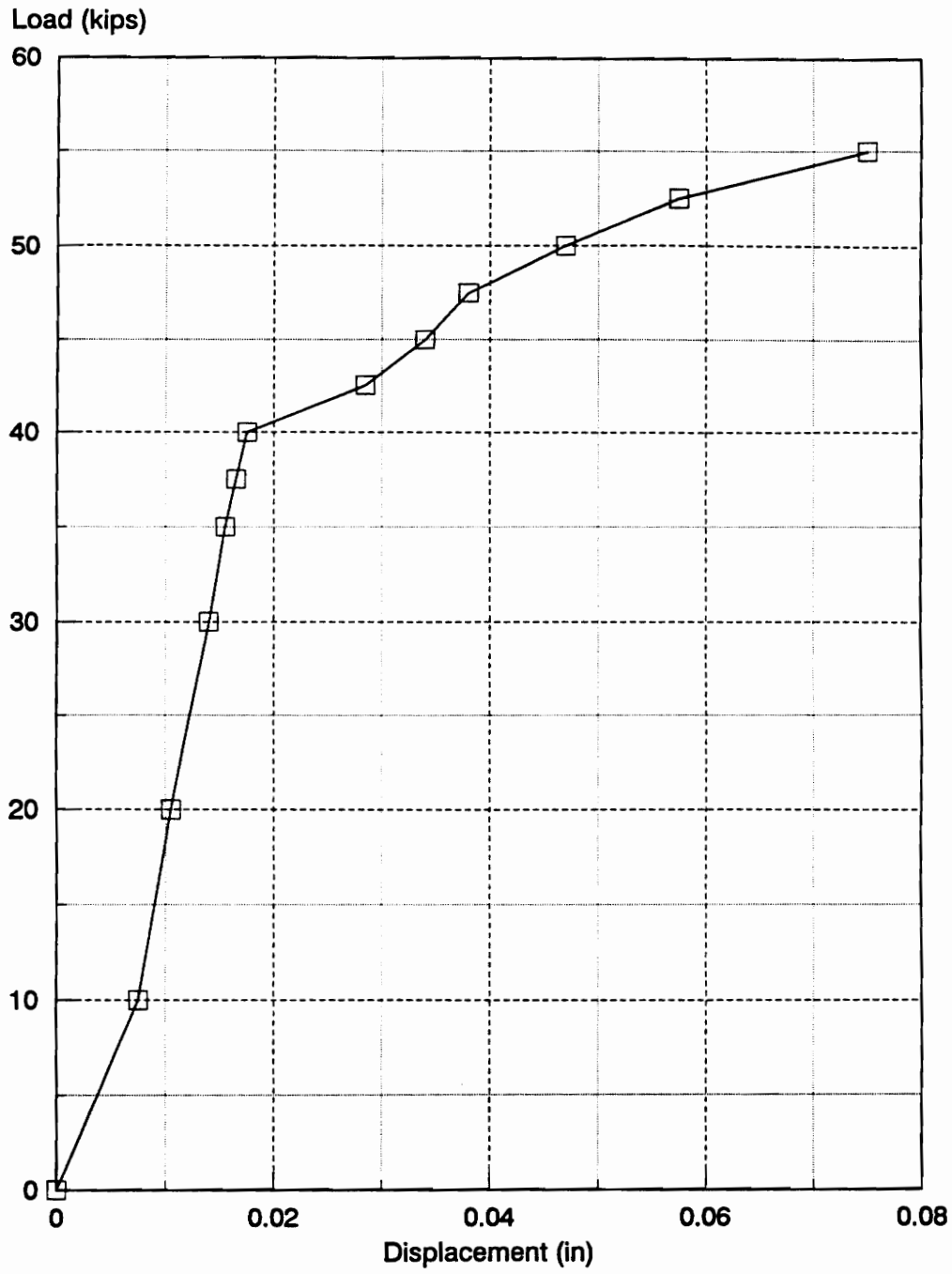

Figure A-1 Load-Displacement for P-L2-2

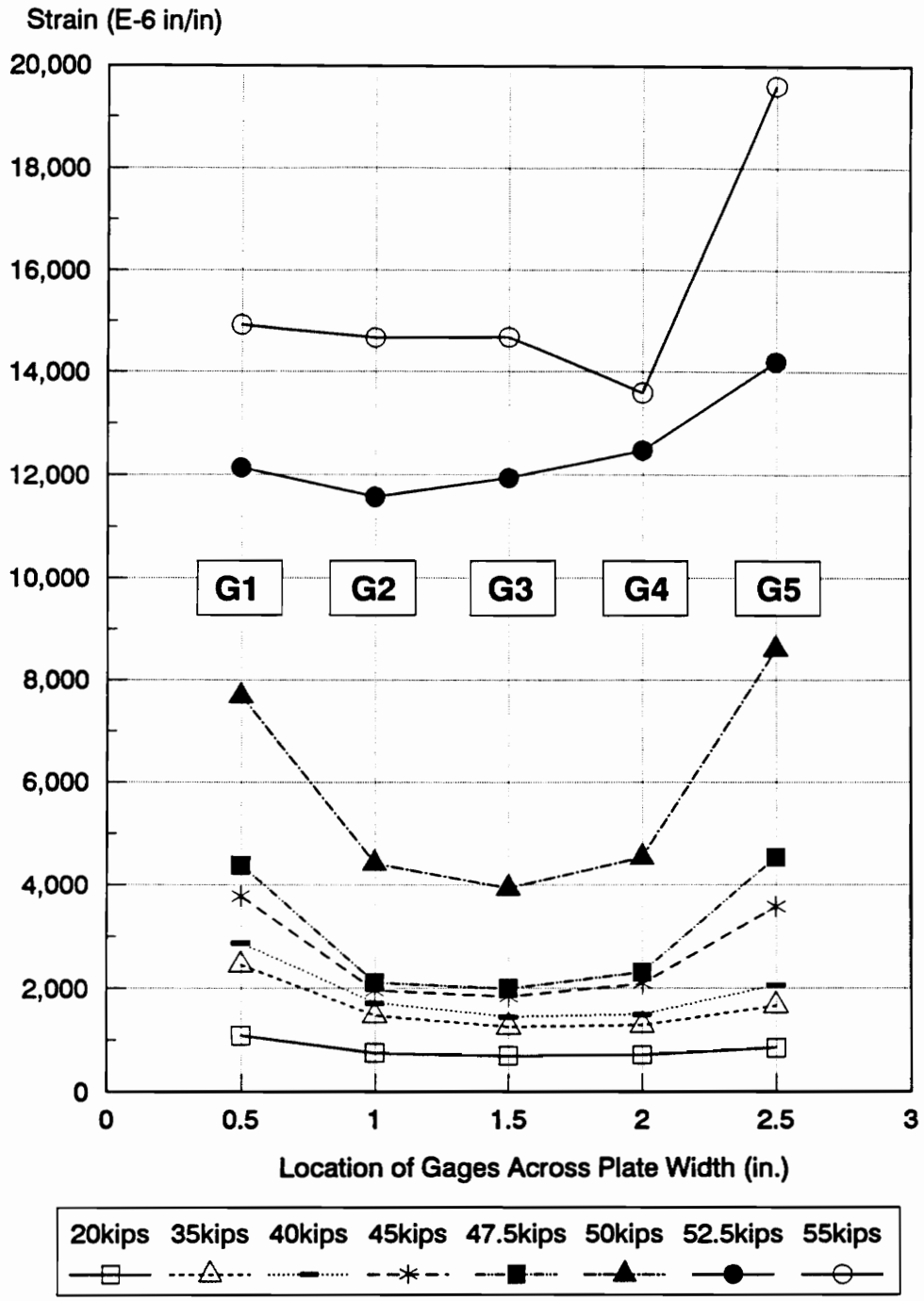

Figure A-2 Experimental Strain Plot Across Plate Width for P-L2-2

Appendix B

ABAQUS Program : The General Model.

```
*NODE
**DEFINE WHOLE PLATE SECTION
**BEGINING
1  ,0.0,0.0
1301,0.0,0.0
13 ,1.5,0.0
**END
1249,0.0,12.0
1261,1.5,12.0
**DEFINE WELDED SECTION
**LEFT
521 ,0.0,5.
1613,0.0  ,3.0
2213,0.0,3.0
**MID
533,1.5,5.
*NGEN,NSET=INSIDE
1  ,13 ,1
*NGEN,NSET=OUTSIDE
1249,1261,1
*NFILL,NSET=PLATE
INSIDE,OUTSIDE,96,13
*NSET,NSET=NALL,GENERATE
1  ,1261,1
1301,1821,26
1901,2421,26
*NGEN,NSET=NPIN
1301,1821,26
1901,2421,26
*NSET,NSET=EDGE,GENERATE
13 ,1261,13
*NSET,NSET=NENDB1,GENERATE
1250,1260,1
*NSET,NSET=NENDB2
1249,1261
*NSET,NSET=NWANT
13,130,247,364,481,473,477
*NSET,NSET=NWANT1,GENERATE
1249,1261,6
*ELEMENT,TYPE=CPS8
1,1,3,29,27,2,16,28,14
*ELGEN,ELSET=EPLATE
1,48,26,1,6,2,48,1
*ELSET,ELSET=ELWANT
66,67,114,115,162,163,210,211,258,259,
245,249,250,254
*SOLID SECTION,ELSET=EPLATE,MATERIAL=STEEL
0.259
*MATERIAL,NAME=STEEL
*ELASTIC
29E3,0.3
```

```
*PLASTIC
55.03655,0.
55.83419, .015075
55.83419, .015175
58.22708, .017992
63.01287, .027827
66.20339, .037717
68.59629, .047635
70.82965, .057558
72.42492, .067503
73.38207, .07747
74.33923, .087437
74.97734, .097415
75.37615, .107401
75.77497, .117387
76.41307, .127365
76.49283, .137162
76.5726, .14736
76.5726, .15736
76.5726, .16736
76.5726. .17736
76.5726, .18736
76.49283, .197362
76.17378, .207373
75.61544, .217393
74.97734, .227415
73.78089, .237456
72.58444, .247497
71.62728, .25553
0.0001, .25554
*BOUNDARY
NPIN,1,2
*BOUNDARY
EDGE,XSYMM
*EQUATION
2
1249,2,1.,1250,2,-1.
2
1250,2,1.,1251,2,-1.
2
1251,2,1.,1252,2,-1.
2
1252,2,1.,1253,2,-1.
2
1253,2,1.,1254,2,-1.
2
1254,2,1.,1255,2,-1.
2
1255,2,1.,1256,2,-1.
2
1256,2,1.,1257,2,-1.
```

```
2
1257,2,1.,1258,2,-1.
2
1258,2,1.,1259,2,-1.
2
1259,2,1.,1260,2,-1.
2
1260,2,1.,1261,2,-1.
**----------------------------------------SPRING PART
*ELEMENT, TYPE=SPRING2,ELSET=G111
301,1  ,1301
321,521 ,1821
*ELGEN,ELSET=SPRG1
301,21,26,1,1
*ELEMENT,TYPE=SPRING2,ELSET=G222
401,1  ,1901
421,521,2421
*ELGEN,ELSET=SPRG2
401,21,26,1,1
*SPRING,ELSET=SPRG1
1,1
246.19
*SPRING,ELSET=SPRG2
2,2
246.19
**----------------------------------GENERATE ALL ELEMENT
*ELSET,ELSET=EALL,GENERATE
1,288,1
301,321,1
401,421,1
**THIS COMPLETES DEFINITION OF STRUCTURE
*STEP,CYCLE=10, INC=100
*STATIC,PTOL=0.1,RIKS
.9,1.,0.1,.9,5.,1261,2,1.
*CLOAD
NENDB1,2,1.852
NENDB2,2,.926
**-----------------------------------------------------EL PRINT
**EL PRINT,ELSET=ELWANT,SUMMARY=NO,POSITION=AVERAGED AT NODES
E22
**EL PRINT,ELSET=ELWANT,SUMMARY=NO,POSITION=AVERAGED AT NODES
**S22
**-------------------------------------------------EL FILE
**EL FILE,ELSET=EALL
**E
**-------------------------------------------------NODE FILE
**NODE FILE, NSET=NALL
**U,CF
**-------------------------------------------------NODE-PRINT
*NODE PRINT,NSET=NWANT,SUMMARY=NO
U2,CF2
```

```
*NODE PRINT, NSET=NWANT1,SUMMARY=NO
U2,CF2
*END STEP
```

Vita

Yun Ping Wang was born in Ping-Tung, Taiwan in September of 1964. He graduated from Chung Ching Institute of Technology with a Bachelor of Science degree in Civil Engineering in July 1986. He then became a military engineering officer and served in the army engineering academy. Three years later, he became qualified to study for an advanced degree abroad. In August 1990, he came to Virginia Polytechnic Institute and State University for his graduate education. He did not only learn the course content from the faculty but also the proper attitude for studying. For him, studying in Virginia Tech was an unforgettable experience. He is planning to continue his engineering officer career in his country until he acquires another opportunity to study.